ADDIS ABABA UNIVERSITY

COLLEGE OF HEALTH SCIENCES

SCHOOL OF PHARMACY

DEPARTMENT OF PHARMACEUTICS AND SOCIAL PHARMACY

GREEN SYNTHESIZED SILVER NANOPARTICLES FOR CIPROFLOXACIN DELIVERY AGAINST RESISTANT *ESCHERICHIA COLI*

BY

MULUALEM WORKYE TAREKEGN

DECEMBER, 2021

ADDIS ABABA, ETHIOPIA

Green Synthesized Silver Nanoparticles for Ciprofloxacin Delivery against Resistant *Escherichia Coli*

BY

Mulualem Workye Tarekegn

A Thesis Submitted to the Department of Pharmaceutics and Social Pharmacy, School of Pharmacy, College of Health Sciences, Addis Ababa University, in Partial Fulfillment of the Requirements for the Degree of Master of Science in Pharmaceutics

Under the Supervision of

Gebremariam Birhanu (PhD), Department of Pharmaceutics and Social Pharmacy, School of Pharmacy, Addis Ababa University and Eyobel Mulugeta (PhD), Technology and Innovation Institute of Ethiopia

December, 2021

Addis Ababa, Ethiopia

Addis Ababa University

School of Graduate Studies

This is to certify that the thesis prepared by Mulualem Workye Tarekegn, entitled: 'Green Synthesized Silver Nanoparticles for Ciprofloxacin Delivery against Resistant *Escherichia Coli'* and submitted in partial fulfillment of the requirements for the degree of Master of Science in Pharmaceutics complies with the regulations of the University and meets the accepted standards with respect to originality and quality.

Approved by:

Name	**Signature**	**Date**
1. Dr. Gebremariam Birhanu (Advisor)	…….	…….
2. Dr. Eyobel Mulugeta (Advisor)	……	…….
3. Dr. Getahun Paulos (External Examiner)	…….	……...
4. Mr. Fentahun Molla (Internal Examiner)	…….	……...

……..

Head of Department

ACKNOWLEDGEMENTS

I am delighted to glorify the Almighty God and his mother, Virgin Saint Mary who gave me strength and patience to accomplish my postgraduate study.

I am honored, to express my deepest gratitude to my advisors Gebremariam Birhanu (PhD) and Eyobel Mulugeta (PhD) for their unreserved and invaluable support throughout this thesis work.

I would like to thank Ethiopia biotechnology institute for providing me the necessary materials for my laboratory activities.

I extend my heartfelt appreciation and thanks to Cadila Pharmaceutical (Ethiopia) PLC for their hospitality and generous donation of standard ciprofloxacin hydrochloride.

Many thanks to Microbiology and Parasitology Department, College of Health Sciences, Addis Ababa University for allowing me to utilize their laboratory facility.

I am pleased to gratify Wollo University and Addis Ababa University for sponsoring my postgraduate study.

My special appreciation and thanks goes to Mr. Tesfaye Gebre for his optimistic support and providing me the dialysis sack.

I also would like to thanks all the academic and administrative staffs of department of pharmaceutics and social pharmacy for their kind and willing supports throughout the entire work of my thesis.

Last but not least, my appreciation extends to Mr. Mesay Wondaya and all my family and friends who directly or indirectly contribute to this work.

TABLE OF CONTENTS

LIST OF FIGURES

LIST OF TABLES

LIST OF APPENDICES

ACRONYMS

AgNPs: Silver Nanoparticles

AgNPs-Cip: Ciprofloxacin loaded Silver Nanoparticles

AMC: Antimicrobial Consumption

AMR: Antimicrobial Resistance

AST: Antimicrobial Susceptibility Test

CDC: Communicable Disease Control and Prevention

Cip: Ciprofloxacin

CLSI: Clinical and Laboratory Standard Institute

DDD: Defined Daily Dose

E.coli: Escherichia coli

ECDC: European Center for Disease Prevention and Control

EFSA: European Food Safety Authority

EMA: European Medicines Agency

EPHI: Ethiopian Public Health Institute

FCC: Face Centered Cubic

JCPDS: Joint Committee on Powder Diffraction Standards

MWCO: Molecular Weight Cut Off

PDI: Polydispersity Index

ROS: Reactive Oxygen Species

SPR: Surface Plasmon Resonance

UTIs: Urinary Tract Infections

WHO: World Health Organization

ABSTRACT

Ciprofloxacin is clinically important fluoroquinolone, effective against *Escherichia coli* (*E. coli*) infections across the globe. However, many clinical isolates of *E. coli* have emerged as resistant to ciprofloxacin, restricting therapeutic options. Due to the paucity of new antimicrobial agents in the drug development pipeline, it is imperative to develop new alternative approaches that improve antibacterial efficacy of the available antibiotics. The aim of the current study was therefore to biosynthesize silver nanoparticles (AgNPs) using aqueous extract of *Aloe camperi* for ciprofloxacin delivery, thereby enhancing its efficacy against ciprofloxacin resistant *E.coli*. In this study, the aqueous extract of *Aloe camperi* was utilized as a reducing and capping agent for the synthesis of AgNPs. Crucial operational parameters were controlled. Ciprofloxacin was loaded on the surface of AgNPs and the encapsulation efficiency was determined. Free and ciprofloxacin loaded particles were characterized by VU-visible spectroscopy, fourier-transform infrared, dynamic light scattering, scanning electron microscope, X-ray diffraction and simultaneous differential scanning calorimeter-thermogravimetric analysis. The *in vitro* release profile of ciprofloxacin from the surface of AgNPs was investigated. Furthermore, the *in vitro* susceptibility test of the loaded particles as compared to its individual components was evaluated by employing disk diffusion test. The results of characterizations revealed a successful synthesis of crystalline AgNPs with an average hydrodynamic diameter of 98.9 nm ± 0.3. Ciprofloxacin was also effectively loaded on the surface of AgNPs with a maximum encapsulation efficiency of 60.94 %. The *in vitro* releasing profile of ciprofloxacin exhibited a biphasic pattern at all study pH conditions. However, the releasing rate was pH dependent. After loading, the susceptibility of *E.coli* against ciprofloxacin was transformed from resistant to intermediate. Therefore, this study demonstrated that biosynthesized AgNPs using *Aloe camperi* aqueous extract could be a potential nano carrier for ciprofloxacin delivery to enhance its efficacy against ciprofloxacin *resistant E.coli*.

Keywords: Aloe camperi, antimicrobial resistance, ciprofloxacin, *E. coli*, functionalized silver nanoparticles, green synthesis, and silver nanoparticles

1. INTRODUCTION

1.1. Overview of antimicrobial resistance

Antimicrobials (including antibacterial, antiviral, antifungal and antiparasit) are medicines used to prevent and treat infections in humans, animals and plants. In general, an antimicrobial is any substance of natural, semi-synthetic or synthetic origin that kills or inhibits the growth of microorganisms with little or no damage to the host. The discovery of antimicrobial agents is arguably one of the greatest achievements of mankind. Without effective antimicrobials, the success of modern medicine in treating infectious disease is unthinkable. While, antimicrobials have played a critical role in preventing and treating many life threatening infections, their utilizations has been exponentially increased. This overuse of antimicrobials accompanied by many sorts of misuse leads to the rapid development and spread of microbial resistance (Vila *et al.*, 2016). Studies reported the correlation between antimicrobial consumption (AMC) and antimicrobial resistance (AMR). For example, significant associations between AMC of fluoroquinolones and AMR of *Escherichia coli* was demonstrated in the second joint report of European Center for Disease Prevention and Control (ECDC), European Food Safety Authority (EFSA) and European Medicines Agency (EMA) (ECDC/EFSA/EMA, 2017). Despite of wide intra- and inter-regional variation in the classes and total amount of antibiotics consumption, World Health Organization (WHO) reported the overall global consumption of antibiotics which ranged from 4.4 to 64.4 Defined Daily Doses (DDD) per 1000 inhabitants per day (WHO, 2018). The consumption has escalated through time especially, across low- and middle-income countries. In this context, Klein and collogues assessed the global antimicrobial consumption pattern between 2000 and 2015, and the result indicated that antibiotic consumption increased by 65%, while the antibiotic consumption rate increased by 39% (Klein *et al.*, 2018). Hence, unlike any other class of drugs, antibiotics have a limited lifespan of utility due to rapid development of AMR through time (Wright, 2011).

AMR which includes antibacterial, antifungal, and antiviral resistances is the ability of a microbe (germ) to resist against the killing and inhibiting effects of a drug (CDC, 2019). It is inherited ability of microorganisms to grow at high concentrations of an antimicrobial, irrespective of the duration of treatment, and is quantified by the minimum inhibitory concentration of the particular antibiotic (Brauner *et al.*, 2016).

AMR has become ever-escalated global health care crisis in the effective prevention and treatment of diversified range of infections caused by bacteria, parasites, viruses and fungi. WHO has declared that AMR is one of the top 10 global public health threats facing humanity. It also reported that antibiotic resistance causes an estimated 700,000 deaths each year globally (WHO, 2014). An estimated annual societal cost for the treatment of antibiotic-resistant infections is about 20 billion USD (Kobayashi *et al.*, 2016). Moreover, WHO also warned that the burden will escalate in over 10 million deaths per year and over 100 trillion dollar in health care system by 2050 unless significant measure is initiated (WHO, 2014). Even though bacterial resistance to conventional antibiotics has been alarmingly increased, the discovery of new alternative antibiotics for the resistant pathogens had been reduced for many decades. This causes high mortality and morbidity rate in patients and significant economic burden on the health sector over the globe (Hay *et al.*, 2018, Willyard, 2017, Alkawareek *et al.*, 2019, Zou *et al.*, 2018). More recently, the United States Communicable Disease Control and Prevention (CDC) reported that antibiotic resistant bacteria and fungi caused more than 2.8 million infections and 35,000 deaths in the US each year (CDC, 2019). The true extent of AMR in the Africa continent has not fully recognized, due to the lack of comprehensive, complete and well recorded national surveillance on antibiotic drug resistance in all countries of the region (WHO, 2014).

AMR is a natural process through which the resistance gen is exploited and horizontally transferred. A plethora mechanism of antibiotic resistances have been identified, including modification of a drug target, molecular bypass, active efflux (or decreased entry), and chemical modification of the compound. Usually, bacteria can inherent several distinct resistance mechanisms against a single class of antibiotic (Wright, 2011).

According to European Commission, more than 70 % of bacteria which caused intra-hospital infectivity were found to be resistant to at least one antibiotic structure (Doma *et al.*, 2020). Among all, gram negative bacteria (GNB), including *E. coli*, have taken a lion share of microbial resistance causing a myriad of infections (Vila *et al*., 2016).

1.2. E.coli

The isolation and characterization of *E.coli* was first reported by Theodor Escherich in 1885. *E. coli* is a facultative, gram-negative, oxidase-negative, rod-shaped bacterium from the family of Enterobacteriaceae. Over more than a hundred years, *E.coli* was known as a harmless commensal of the gastrointestinal tract in warm-blooded animals. But the

genetically modification enable the microbe to become diversified pathogen (Croxen *et al.*, 2013). Currently, *E.coli* is the most studied microorganism and one of the most common pathogen over the globe that causes many infections including: community and hospital acquired urinary tract infections (UTIs), bloodstream infection, intra-abdominal infections such as peritonitis, neonate meningitis, and food borne infections (Walsh and Collyns, 2017, Vila *et al*., 2016). Among these, UTIs are some of the most common health problems caused by pathogenic *E.coli*. Several investigations reported that *E.coli* is principal cause of UTIs. For example, a study which was conducted in Denmark, reported that the most common uropathogen in patients with uncomplicated- and complicated UTI was *E. coli* which accounted 69 % and 70 %, respectively (Córdoba *et al.*, 2017). Another review also strengthens this epidemiological finding which summarized uropathogenic *E.coli* as the major etiological agent for both uncomplicated- and complicated UTIs which accounts 75 % and 65 %, respectively (Flores-Mireles *et al.*, 2015).

UTIs are the second commonest bacterial infections of human next to respiratory tract infections which causes substantial morbidity and mortality and major economic burden for the societal health care system (Kudinha, 2017). A review on the global prevalence of UTIs, summarized that as health care associated UTI is one of the most common causes of healthcare associated infections and its frequency among healthcare-associated infections is 12.9, 19.6 and 24 % in the United States, Europe and developing countries, respectively (Tandogdu and Wagenlehner, 2016). In Ethiopia, several cross sectional and retrospective studies revealed the high prevalence of UTIs in the country which were predominantly caused by *E.coli*. For instance, the results of each cross sectional study which was conducted at Arsho Advanced Medical laboratory (Bitew *et al.*, 2017), Shashemene referral hospital (Seifu and Gebissa, 2018), and Jimma University Specialized Hospital (Beyene and Tsegaye, 2011), demonstrated the prevalence was 36 %, 90.1 %, 9.2%, respectively. In all study area, the most common isolated pathogen was *E.coli* with 39.3 % and 33.3 % in Shashemene referral hospital and Jimma University Specialized hospital, respectively. Other retrospective chart review studies at Tikur Anbessa Specialized Teaching Hospital (Kabew *et al.*, 2013) and Dessie regional health research laboratory (Abejew *et al.*, 2014) also reported similar results with prevalence of 23.32 % and 27.35%, respectively. In both study institutions the predominant uropathogen was *E. coli* with 44.62% and 60.29%, respectively.

In general, most UTIs are caused by *E.coli* strain which have been successfully treated with fluoroquinolones for long time. For example, in the United States between 2002 and 2011,

nearly half (49 %) of uncomplicated UTIs were treated with fluoroquinolones, mainly ciprofloxacin and levofloxacin (Kobayashi *et al.*, 2016).

1.3. Ciprofloxacin

Ciprofloxacin is the second generation quinolone which is highly effective against gram negative bacteria, including *E.coli* (Deck and Winston, 2012). The original lead compound of quinolone, a 7-chloro-4-quinolone was isolated as a serendipitous offshoot from chloroquine synthesis as a by-product as illustrated in Figure 1 below. It showed anti gram negative bacterial activities. However, its potency and spectrum of activity was not significant enough to be used clinically. After modification of the lead compound, the first commercialized quinolone, nalidixic acid was synthesized by George Lasher and coworkers in 1962. Even though nalidixic acid has many limitations and its utilization is limited for uncomplicated UTIs, its discovery inspired the development of new class of quinolones. After an intensive effort for prolonged time, the discovery of the first fluorinated quinolone (Norfloxacin) was a great breakthrough led to a significant improvement in the activity against gram-negative species. Then after, a little modification at N-1 ethyl of norfloxacin to an N-1 cyclopropyl group led to the discovery of ciprofloxacin (Takahashi *et al.*, 2003, Bisacchi, 2015).

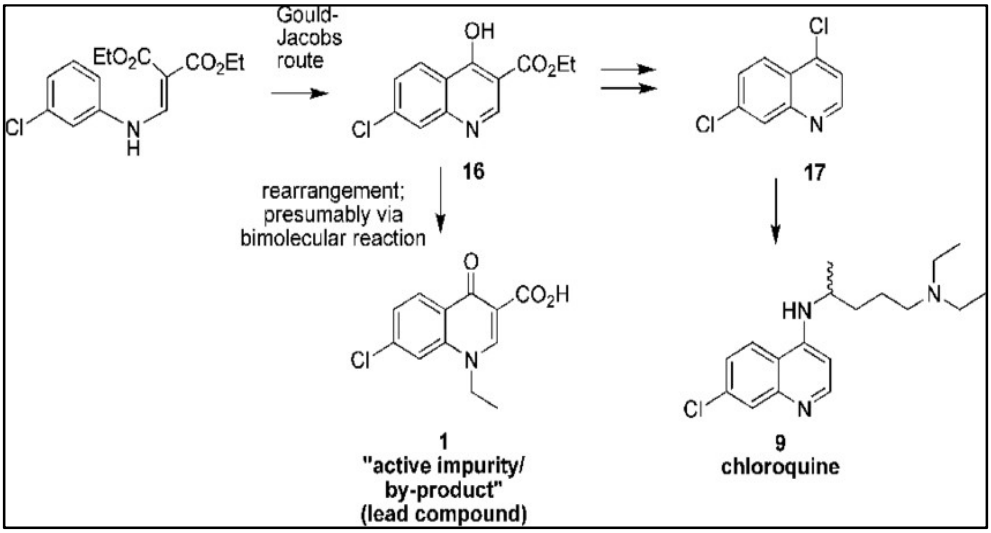

Figure 1: Diagrammatical illustration of chloroquine synthesis and the serendipitous discovery of quinolone lead compound as a by-product. Adopted from Bisacchi, (2015

1.3.1. Physicochemical properties

Ciprofloxacin is zwitterionic molecule that comprises a carboxylic acid group (C-3, pKa_1= 6.1) and an amine group in the piperazine moiety (C-7, pKa_2 = 8.7) as displayed in the Figure 2(a). Hence, it exhibits a pH-dependent biphasic solubility; high solubility at pH values below 5 and above 10, and minimum solubility near the isoelectric point, which is close to neutral. Its pH dependent ionization is illustrated in the Figure 2(b) which significantly affects the electrostatic interaction with other materials. Ciprofloxacin hydrochloride is a salt form which exhibited better solubility at neutral pH and highly soluble at acidic pH. However, at intestinal pH like 6.8 and 7.5, its solubility is far lower (Gu and Karthikeyan, 2005, Olivera *et al.*, 2011, Li *et al.*, 2011).

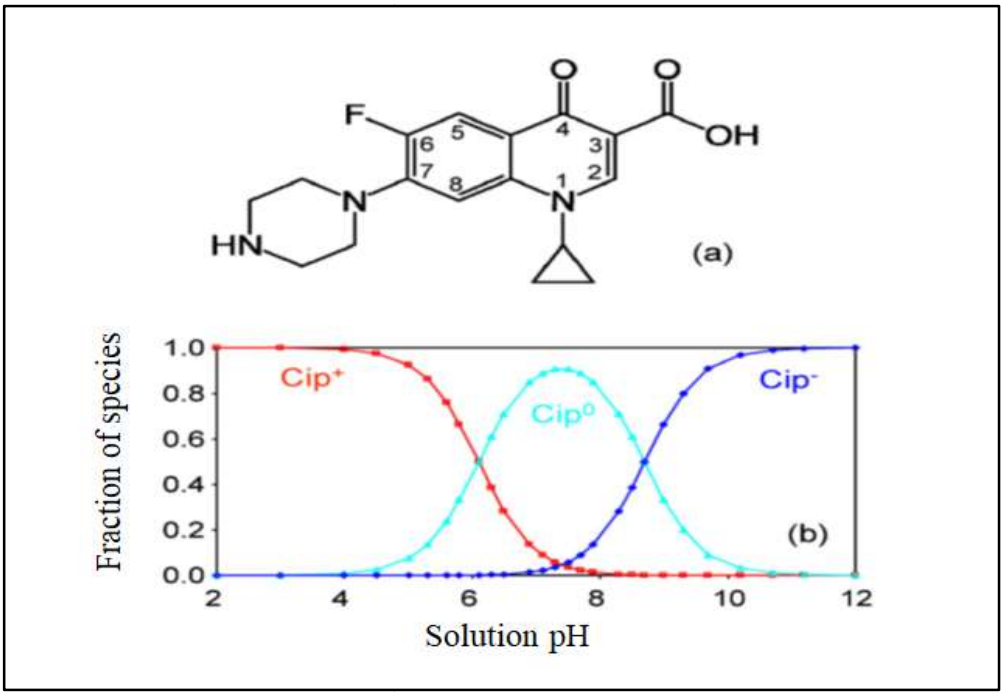

Figure 2: Schematic demonstration of molecular structure (a) and pH dependent ionization (b) of ciprofloxacin molecule. Picture was adopted from Li *et al*., (2011).

1.3.2. Mechanisms of antibacterial activity of ciprofloxacin

Ciprofloxacin as other quinolones inhibits two structurally related members of the topoisomerase class of enzymes in bacterial cell replication processes, namely DNA gyrase and topoisomerase IV. DNA gyrase uniquely catalyzes the introduction of negative superhelical twists into closed covalently circular chromosome and plasmid DNA within the bacterial cell while topoisomerase IV functions to resolve interlinked (catenated) daughter

DNA molecules that result from replication of circular DNA, to allow their segregation into daughter cells. Both enzymes are essential for cellular replication. Hence, quinolones act, preventing both DNA from introducing the negative superhelical twist into its strands and decatenation of the daughter cells (LeBel, 1988, Jacoby *et al.*, 2015).

1.3.3. Clinical applications of ciprofloxacin

Ciprofloxacin has been used as a common antibiotic for many types of infections, like UTIs worldwide since its first approval by the United States Food and Drug Administration (FDA) in 1987 in the form of ciprofloxacin hydrochloride tablet and oral suspension (FDA, 2016, Olivera *et al.*, 2011). Moreover, according to the Ethiopian Standard Treatment Guideline (ESTG) for general hospitals, ciprofloxacin is still one of the first line antibiotic for many common *E.coli* caused hospitals and community acquired infections, including acute uncomplicated UTIs in men and women, acute uncomplicated pyelonephritis in non-pregnant women, sever acute complicated pyelonephritis in men, complicated UTIs in men and bacillary dysentery. It is also used to as a prophylaxis in some surgical procedures such as, upper gastrointestinal tract elective bowel surgery and prostatectomy (EFMHACA, 2013).

1.3.4. Ciprofloxacin resistant *E.coli*

In general, fluoroquinolones are under WHO category of 'critically important antimicrobials' for human medicine (Collignon *et al.*, 2016). Ciprofloxacin is a clinically important fluoroquinolone, effective against *E. coli* infections across the globe. However, many clinical isolates of *E. coli* have emerged resistance to ciprofloxacin, restricting therapeutic options (Bisacchi, 2015, Praski Alzrigat *et al.*, 2021). *E.coli* develops resistance for quinolones through two main mechanisms: (1) by alteration of quinolone targeted Enzymes (Deoxyribonucleic Acid (DNA) gyrase and DNA topoisomerase IV), (2) by expression of drug resistance membrane associated efflux pump systems (Blondeau, 2004, Hooper and Jacoby, 2016)

The rate of spreading of quinolone resistant *E.coli* has increased dramatically through time (Spellberg and Doi, 2015). WHO, in its first report on global antibacterial resistance, also labeled *E.coli* as one of the internationally concern pathogens and fluoroquinolones as one group of common antibacterial drugs against the treatment of this pathogen. According to this report, the pattern of *E. coli* resistance against fluoroquinolones was found to be 50 % or more in all WHO regions; except Europe. Overall percentage range of resistant *E. coli* for

fluoroquinolones from the national data of 14 WHO Africa region countries was 14 % (Lesotho) to 71 % (Ethiopia) (WHO, 2014).

Recently, Ethiopian Public Health Institute (EPHI) collaborated with international partners, has conducted first phase national antimicrobial surveillance since September 2017 on six clinical sites, including Tikur Anbesa Specialized Hospital. As the finding revealed that the most common pathogen isolated at Tikur Anbesa Specialized Hospital during the study period was *E. coli.* Out of which, 67 % was found to be resistant against ciprofloxacin (EPHI, 2020). This is sound higher than the expected general frequency of emerging resistant bacterium to ciprofloxacin (frequency of between $< 1\times10^{-9}$ to $1x10^{-6}$) (FDA, 2016).

This implies, resistance to ciprofloxacin generally limits the available antibiotic options. Moreover, countries like, Ethiopia will lose the first line accessible antibiotic for the treatment of common infections which may result in increasing the economic burden on the health care system due to prolonged course of treatment and searching other expensive alternatives, even escalating the morbidity and mortality. Therefore, in this era at which the discovery of new alternative antibiotics has been declined, developing new alternative approaches to preserve and / or improve antibacterial efficacy of the available antibiotics is a priority research area in order to cope the problem (Alkawareek *et al.*, 2019, Allahverdiyev *et al.*, 2011).

Due to their powerful bactericidal effects, metallic nanoparticles like, silver, copper, titanium, zinc, magnesium and gold nanoparticles have become a promising therapeutic template to circumvent bacterial resistance. Among these, silver nanoparticles (AgNPs) showed a strong antibacterial effects (Rai *et al.*, 2012).

1.4. Silver nanoparticles

Silver utilizations in different fields has a long history due to its unique physicochemical properties like high electrical and thermal conductivity, low melting and boiling point, high reactivity and antimicrobial activities. Silver in the form of nanoparticles revealed even more unique properties, which enables it to be utilized in multiple fields of technique and medicine (Pryshchepa *et al.*, 2020). Despite there is no clear data available on the historical production of AgNPs, the first report was from Lea in 1889. He reported the synthesis of citrate stabilized colloidal silver nanoparticles (Nowack *et al.*, 2011, Lea, 1889). Then after, the effectiveness of AgNPs against medically relevant microorganisms, including bacteria,

viruses, fungi and yeasts, has been assessed by many researchers. Their profound antimicrobial activities and unique physicochemical characteristics inspire the development and utilization of new and performance-enhanced nanosilver-based biomedical products such as, wound dressing, orthopedic materials, bandages, antiseptics, catheters, anticancer agents and drug deliver platforms (Burdușel *et al.*, 2018, Abbas *et al.*, 2018).

1.4.1. Physicochemical properties of AgNPs

Unlike the bulk material, the size, shape and morphology of the nanoparticles significantly determine the surface area-to-volume ratio which in turn changes their physical, chemical and biological properties (Chouhan, 2018). AgNPs have unique physicochemical properties, including but not limited to: impressive optical-, electrical-, thermal- and catalytic properties which are superior to their corresponding bulk material (Zhang *et al.*, 2016). Other properties of AgNPs, including, surface functionalization, agglomeration and surface charge also significantly affect their biological activities and safety (Gomes *et al.*, 2021).

AgNPs exhibit a definite optical property due to the surface plasmon resonance (SPR) which consists of a collective oscillation of conduction electrons excited by the electromagnetic field of light (García, 2011). When the size of a metallic particle is reduced to a few nanometers, the optical properties are dramatically modified by the appearance of surface plasmon and its resulting behavior is completely different from the bulk metal one. Since in bulk metal, the valance and conduction electrons overlapped one over the other which do not allow electrons move freely. But in the case of nanoparticles, the valance and conduction electrons neither far apart, like in the case of a single atom nor overlap, like in the case of bulk metal. Rather they exist in close due to large electron density as illustrated in Figure 3. This property is very crucial and commonly employed for identification and qualitative determination of the relative quality of AgNPs (like size, shape and polydispersity) during synthesis (Abbas *et al*., 2018, Chouhan, 2018, Qureshi, 2013).

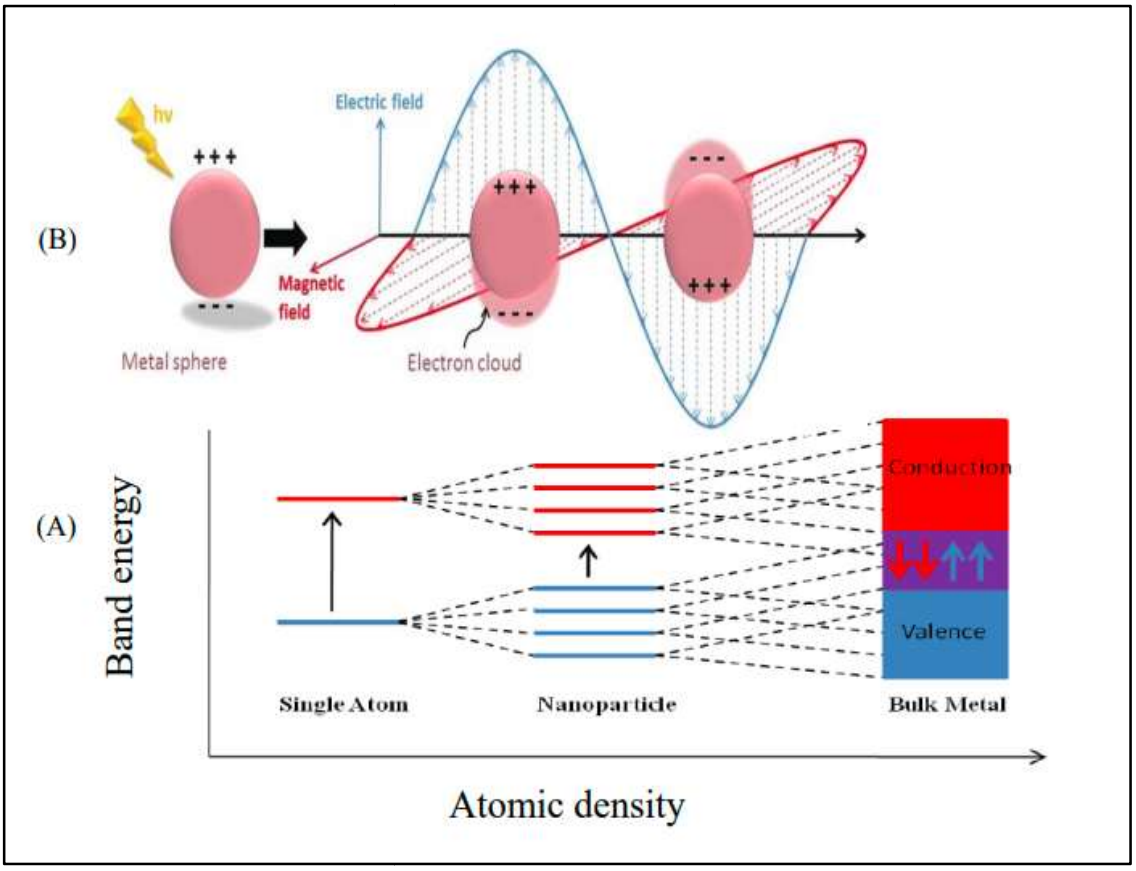

Figure 3: Schematic illustration of (A) conduction and valence electron bands for single atom, nanoparticles and bulk metal (Qureshi, 2013), (B) the interaction of electromagnetic energy with conduction electrons on the surface of AgNPs (Peiris *et al.*, 2016).

1.4.2. Applications of AgNPs as antibacterial agents

AgNPs have been extensively studied and recognized as promising tools in therapeutics due to their suitable properties, including high surface-to-volume ratio, ease of synthesis, tunable surface chemistry and surface functionalization, and good penetration in the organism (Gomes *et al.*, 2021).

Despite the fact that the effects of AgNPs depend on various factors including size (Shameli *et al.*, 2012), shape (Rout *et al.*, 2014), surface charge and colloidal states (Jelinkova *et al.*, 2019, Ivanova *et al.*, 2018), they are significantly more toxic than Ag^+ to prokaryotic cells and have been shown to be effective bactericides at nanomolar concentrations, compared with micromolar levels for Ag^+ (Stensberg *et al.*, 2011, Durán *et al.*, 2010, Lok *et al.*, 2006, Ibrahim, 2015, Li *et al.*, 2017). Even though AgNPs has been widely applied in wound dressing and catheter coating during surgery to prevent the biofilm formation (Roe *et al.*,

2008, Jelinkova *et al.*, 2019), their applications as antimicrobial agents is restricted, due to their dose dependent toxicity (Akter *et al.*, 2018). But many studies reported that small dose of AgNPs induced little or no damage to animal tissues (Sung *et al.*, 2009, Sung *et al.*, 2011, Hadrup and Lam, 2014). For example, the *in vivo* toxicity of AgNPs-incorporated preparations over more than two thousands animal studies revealed minimal induction of secondary markers of liver damage even in the presence of chronic oral AgNPs doses greater than 300 mg/kg/day for 28 days (Ivanova *et al*., 2018, Kim *et al.*, 2008). Furthermore, an *in vivo* human time-exposure study of orally dosed commercial AgNPs was conducted on 60 healthy subjects of both sexes, aged 18 to 80 years. The subjects were treated with a single daily dose of 2.5 or 7.9 µg/kg body weight based on a 60 kg adult for 3,7 or 14 days. The results demonstrated that there were no clinically relevant changes in body weight, blood pressure, metabolic markers or cellular composition of blood in any group (Munger *et al.*, 2014). On the bright side, many studies showed that the combination of AgNPs with common antibiotics brought two important benefits: (1) It reduced the side effects of both the drug and AgNPs by reducing the required individual doses; (2) It also provides enhanced bactericidal effects. For example, Adil and his collogue evaluated the combined effect of AgNPs synthesized with aqueous extract of *Fagonia indica* and ciprofloxacin against resistant *E. coli*. They found an enhanced effect from the combination as compared to both the ciprofloxacin and AgNPs alone (Adil *et al.*, 2019) Moreover, several other studies signified that antibiotics-functionalized AgNPs could enhance their antibacterial effects against resistant bacteria (Allahverdiyev *et al*., 2011, Jelinkova *et al*., 2019, McShan *et al.*, 2015, Cunha *et al.*, 2016, Adil *et al*., 2019).

1.4.2.1. Mechanism of antimicrobial activity of AgNPs

Despite the exact mechanism of AgNPs has not been elucidated yet, scientists proposed different possible bactericidal actions. The suggested mechanisms include: cell wall lysis, cell membrane disruption, breakage of double stranded DNA, prevents unwind of DNA strands during replication, deplete intracellular adenosine triphosphate (ATP), the production of reactive oxygen species (ROS) and interfere the function of vital enzymes (Lok *et al.*, 2006, Radzig *et al.*, 2013, Tamboli and Lee, 2013, Li *et al.*, 2010, Ivanova *et al.*, 2018). Roy *et al*., (2019) well summarized the general antibacterial mechanisms of green synthesized AgNPs in their review, as illustrated in Figure 4 (Roy *et al.*, 2019) which can be simplified into three primary mechanisms: (1) adhesion of AgNPs on the surface of bacterial cell wall and cell

membrane; (2) penetration of AgNPs inside the cell and disrupted intracellular structures and biomolecules and (3) generation of ROS (Ivanova *et al*., 2018).

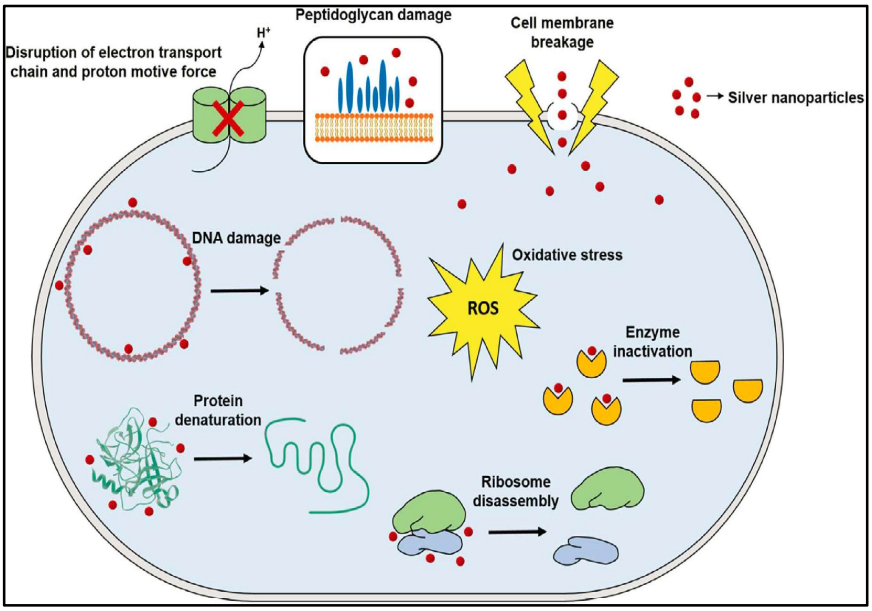

Figure 4: General antimicrobial mechanisms of AgNPs.

1.4.3. Utilization of AgNPs as a drug delivery platform

Delivery of antibiotics by nanoparticles to the site of infection is a promising therapy, particularly for controlled release of drugs, which in turn decreases the dose required to achieve a clinical effect. For this purpose, biodegradable nanoparticles have been commonly employed. But recently, tremendous attention, scientific investigations, and financial support are oriented towards the development of AgNPs-based drug-delivery platforms, due to their intrinsic features, including its capacity to bind a wide range of organic molecules, its tunable surface, large drug payload capacity, and its low toxicity (Burdușel *et al*., 2018, Allahverdiyev *et al*., 2011). AgNPs can also provide additional asset as a drug carrier to facilitate the transportation of hydrophilic compounds like ciprofloxacin hydrochloride (partition coefficient = 0.28) to the bacterial cell membrane. Since bacterial cell membrane is composed of phospholipids and glycoprotein which are hydrophobic groups (Li *et al.*, 2005).

Researchers have investigated the potential interaction of AgNPs with antibiotics through their hydroxyl and amine groups to prepare antibiotic functionalized AgNPs (Jelinkova *et al*., 2019, Takács-Novák *et al.*, 1992, Li *et al.*, 2005). Recently, rational efforts have been paid towards the utilization of plant extract-mediated synthesized AgNPs as drug delivery platform without any surface modification and ligand attachments. This is due to the fact that

in plant extract mediated AgNPs synthesis, surface functionalization is inevitable. Since every aqueous plant extract comprises surplus amount of phytochemicals which have certain affinity to silver surface. Ivanova and colleagues summarized the deriving of this attachment as chemisorption and physisorption phenomena in their review. Chemisorption occurs through ionic, covalent and coordinate covalent bonds. Some elements (like S, O and N) which commonly found in most primary and secondary metabolites have strong affinity to silver surface. While physisorption happens via non-specific, weak Van der Waals forces. After purification, those components having strong sorption remain on the surface. No matter how it is difficult to elucidate the specific responsible biomolecules, those remained adsorbed on the surface act as capping agents as well as ligands for the drug loading (Ivanova *et al*., 2018). In this context, some scientific reports have been published (Sadat Shandiz *et al.*, 2017, Harshiny *et al.*, 2015, Perveen *et al.*, 2018).

1.4.4. Synthesis methods of AgNPs

Owing to their versatile applications of AgNPs in different fields, it is indispensable to look for an eco-friendly and cost-effective production methods which can provide a sustainable supply for the growing demand (Burdușel *et al*., 2018, Ivanova *et al*., 2018). Several methods have been developed for the synthesis of AgNPs. These methods follow either of the two common approaches, namely (1) top-down approach in which the bulk material get downsizing until the required nanostructure is attained, and (2) bottom-up approaches in which Ag^{+} undergone a chemical or biological reduction by organic or inorganic agents that leads to the formation of Ag^{o} nuclei and subsequent oligomeric agglomeration and growth of AgNPs. Synthesis methods can also be broadly categorized into three techniques based on the processes employed, namely physical, chemical and biological methods (Pryshchepa *et al*., 2020). Each method has its own prone and cons that related to the common challenges of production cost, stability, scalability, uniform particle size, size distribution and environmental pollution (Jamkhande *et al.*, 2019, Parveen *et al.*, 2016).

1.4.4.1. Physical method

The principle of physical method is disincorporation of the bulk material to fabricate the required nanostructure in the top-down approach. In this method the physical agents, such as heat, electrical discharge, plasma, or electromagnetic, irradiation are employed to produce the nanoparticles. Evaporation-condensation and laser ablation are the two most common physical AgNPs synthesis methods. The former processes could be carried out in a tube

furnace at atmospheric pressure which need large amount of energy and time while the later utilizes laser as an energy source to remove surface atoms from solid metal (Kim *et al.*, 2017). Other less commonly practiced physical methods, including thermal decomposition from the Ag^{+} complex, employing the electrical discharge machining without addition of any surfactants, direct metal sputtering into the liquid medium were also reported. Even though, the common physical methods able to synthesize large quantity of AgNPs with high purity without environmental hazard, they require special equipment, high power consumption and long time for synthesis. All these increase the production cost. Moreover, as capping agents are not incorporated, particles agglomeration is usually a great challenge (Lee and Jun, 2019, Pryshchepa *et al.*, 2020, Iravani *et al.*, 2014).

1.4.4.2. Chemical method

The chemical synthesis of AgNPs is a bottom-up approach in which Ag^{+} ion undergone a chemical reduction by organic or inorganic agents that leads to the formation of colloidal silver metal particles which is followed by agglomeration into oligomeric clusters (Patra and Baek, 2014, Dada *et al.*, 2018). The chemical reduction of metal ions has been the most universal and easy route for the production of the metal nanoparticles for long period of time. This process comprises three common components, namely (1) metal precursor, like $AgNO_3$ $AgClO_4$, AgCl, (2) reducing agents, like $NaBH_4$, sodium citrate, glucose, N,N-dimethyformamide and (3) stabilizing or capping agents (Chouhan, 2018).

Four common chemical reactions are employed in the chemical synthesis of AgNPs: (1) Citrate reduction: in this method $AgNO_3$ used as metal precursor while trisodium citrate is utilized as the reducing, capping and stabilizing agent. (2) Borohydride reduction: the most popular among other chemical methods. The popularity of $NaBH_4$ for Ag NPs production comes from the fact that it has higher reducing capability than citrate. (3) Tollens reaction: a less popular chemical method which employs Tollen's reagent, $Ag(NH3)_2OH$ as a precursor, and the aldehyde-group containing reducing agent. (4) Polyol process which involves the reduction of silver nitrate with ethylene glycol in the presence of the capping agent polyvinylpyrrolidone, In this case, ethylene glycol served as both reducing agent and solvent (Pryshchepa *et al.*, 2020) .

Generally chemical synthesis methods are expensive. Most of the chemicals utilized for reduction, capping and stabilization are environmentally hazardous (Ivanova *et al.*, 2018, Lee and Jun, 2019).

1.4.4.3. Green method

Green synthesis is a bottom-up approach, in which Ag^+ is reduced and stabilized with the help of biological agents from bacteria, fungi, algae, and plants. This method does not require in utilizing environmental hazardous chemicals for the reduction and stabilization processes. In this context, many researchers successfully synthesized AgNPs by employing different species of microorganisms and plants for different purposes (Sun *et al.*, 2014, Selvan *et al.*, 2018, Ahamed *et al.*, 2011).

Microorganisms based AgNPs synthesis is ecofriendly and cost effective method as compared to physical and chemical methods. Microorganisms, including bacteria and fungi have been extensively studied for AgNPs synthesis (Singh *et al.*, 2016). The bacteria and fungi based AgNPs synthesis is mainly based on the reduction of Ag^+ to Ag^0 by enzymes, like nitrate reductase. This method requires a complex steps for microbial sampling, isolation, culturing and purification. Furthermore, it provides lower yield as compared to plant extract-mediated synthesis (Prabhu and Poulose, 2012).

Among all the above nanoparticles syntheses methods, plant extract-mediated green synthesis of AgNPs has become the most popular, due to its ecofriendly nature, accessibility, scalability, less time consuming and reduces the cost of microorganism isolation and culture media (Otunola *et al.*, 2017). However, the exact mechanism as well as the phytochemical components responsible for the reduction and stabilization in plant based AgNPs synthesis have not been elucidated yet, both primary metabolites (carbohydrate, protein, amino acids) and secondary metabolites, like flavonoids, alkaloids, polyphenols, terpenoids are suggested to be involved. In this context, many researchers synthesized AgNPs with different medicinal plants extract and evaluated their antibiotic effects (Lavanya *et al.*, 2013, From, 2016, Malapermal *et al.*, 2017, Sangeetha *et al.*, 2014, Bonde, 2011, Ibrahim *et al.*, 2019, Sanchooli *et al.*, 2018).

One of the big challenges for plant extract-mediated AgNPs synthesis is lack of homogeneity across the produced nanoparticles. Hence, researchers have tried to control the reaction conditions for producing homogenous nanoparticles (Singh *et al*., 2016). The influence of parameter controlling is diagrammatically demonstrated in Figure 5. No matter what method is employed for the synthesis of AgNPs, there are some crucial operational parameters, including silver ion concentration, volume ratio of reactant, temperature of reaction, pH of the medium and reaction time that influence the rate of synthesis, the size and size

distribution of the nanoparticles. Hence, to produce a better quality of nanoparticles these factors have to be controlled (Dada *et al*., 2018). Researchers commonly used to vary one operational variable at a time to evaluate the influence of each factor on the quality of synthesized nanoparticles (Raj *et al.*, 2020, Benakashani *et al.*, 2016, Ulaeto *et al.*, 2019).

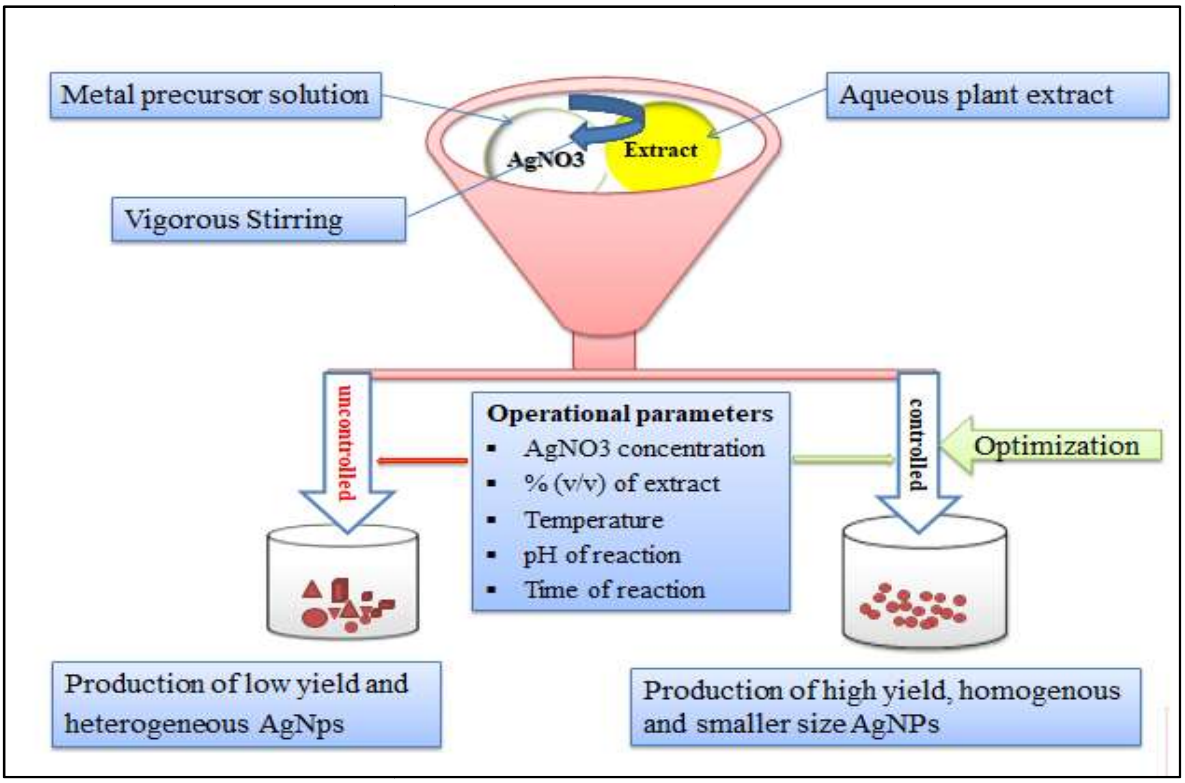

Figure 5: Schematic diagram demonstrates plant extract mediated synthesis of AgNPs.

Controlling the operational parameters can provide high yeild and monodispersed nanoparticles while hetrogeneous particles will be produced in uncontrolled conditions (Singh *et al*., 2016).

1.5. Aloe camperi

Aloes are perennial plants that comprise herbs, shrubs and trees which belonging to the family of Aloeceae. The genus mainly distributed across sub-Saharan Africa, which accounts 90 % of the total taxa. Forty six species of Aloes are recognized in the flora of Ethiopia out of which 24 Aloe species are endemic to Ethiopia (Adom *et al.*, 2020, Oda and Erena, 2017, Megeressa *et al.*, 2015). *Aloe camperi* Schweinf (local name Eret) is perennial, succulent, shrubby medicinal plants which is an endemic in the north-central highland of Ethiopia (extends from northern Shewa towards Eritrea). The image of *Aloe camperi* is displayed in

Figure 6 below. It is characterized by its erect, ascending and sprawling stem, with rosette leaves which grows in cluster. The leaves grow up to 60 cm long and reach up to 15 cm width at the base which contain the whitish spot on it (Demissew *et al.*, 2001, Abbas *et al*., 2018). It has been used as a traditional medicine for skin burns, dandruff, stomach pain and hair fails. The aqueous extract of *Aloe camperi* comprises steroids, alkaloids, phenols, tannis, flavonoids, glycosides, carbohydrate and terpenoids (Demoz *et al.*, 2015, Medhin *et al.*, 2019) which have been suggested to be involved in reduction and stabilization for metal nanoparticles synthesis. As to my knowledge, no study has been done on the *Aloe camperi* aqueous leaf extract mediated AgNPs synthesis for drug loading and antibacterial activities yet.

Figure 6: Image of *Aloe camperi* Schweinf (Eret). (Picture was taken from the collection area by Mulualem W. in Nov, 2021).

1.6. Significant of the study

The impact of AMR on the global health care system has been worsen through time while the discovery of new antibiotics has been negligible to catch the pace of resistance (WHO, 2014). Gram negative bacteria (GNB), including *E. coli*, have taken a lion share of the whole

microbial resistance that cause a myriad of infections. Among these, UTI is one of the commonest group of bacterial infection of human all over the globe which causes substantial morbidity, mortality and major economic burden for the societal health care system (Kudinha, 2017, Tandogdu and Wagenlehner, 2016, Flores-Mireles *et al*., 2015, Vila *et al*., 2016). Different literatures also reported the high prevalence of UTI in Ethiopia (Bitew *et al*., 2017, Seifu and Gebissa, 2018).

The principal cause of UTI is *E.coli* (Córdoba *et al*., 2017) which have been successfully treated by ciprofloxacin for a long time. However, many clinical isolates of *E. coli* have emerged as resistant to ciprofloxacin, restricting therapeutic options (Bisacchi, 2015, Praski Alzrigat *et al*., 2021). Moreover, countries like, Ethiopia will lose the first line accessible antibiotic for the treatment of common UTIs which may result in elevation of the total health care cost due to the prolonged course of treatment and searching other expensive alternatives, even escalating in morbidity and mortality (EFMHACA, 2013).

Therefore, due to the paucity of new antimicrobial agents in the drug development pipeline, it is imperative to develop new alternative approaches that preserve or improve antibacterial efficacy of the available antibiotics in order to circumvent the problem (Alkawareek *et al*., 2019, Allahverdiyev *et al*., 2011, Soucy *et al.*, 2020). In this context, the profound antimicrobial activities of AgNPs have inspired the development and utilization of new and performance-enhanced nanosilver-based biomedical products (Burdușel *et al*., 2018, Abbas *et al*., 2018). Many researchers synthesized AgNPs using different medicinal plants extracts and evaluated their antimicrobial effects with a promising results (Lavanya *et al*., 2013, From, 2016, Malapermal *et al*., 2017, Sangeetha *et al*., 2014, Bonde, 2011, Ibrahim *et al*., 2019, Sanchooli *et al*., 2018). Different studies also reported the improved bactericidal effects due to the combination of AgNPs with common antibiotics (Jelinkova *et al*., 2019, Adil *et al*., 2019). Moreover, AgNPs are suitable drug-delivery platforms, due to its intrinsic features, including its capacity to bind a wide range of organic molecules, its tunable surface, large drug payload capacity, and its low toxicity (Burdușel *et al*., 2018, Allahverdiyev *et al*., 2011, Munger *et al*., 2014).

Besides this, green synthesis of nanoparticles is simple, accessible, environmental benign, facile and cost effective (Otunola *et al*., 2017). Furthermore, the drug loading processes on biosynthesized AgNPs does not need any additional surface modification and ligand

attachment (Sadat Shandiz *et al*., 2017, Harshiny *et al*., 2015) which is simple and efficient method.

Ethiopia is well endowed with several species of medicinal plants. *Aloe camperi* is one of an endemic perennial, shrubby medicinal plant of Ethiopia (Adom *et al.*, 2020, Megeressa *et al*., 2015, Demissew *et al*., 2001). Its aqueous extract comprises many groups of phytochemicals which could be utilized as reducing and stabilizing agents in green synthesis of AgNPs (Demoz *et al*., 2015). As to my knowledge, no study has been reported on the *Aloe camperi* aqueous leaf extract mediated AgNPs synthesis for antibiotic drug delivery yet.

The rationale of the current study was therefore to biosynthesize AgNPs using aqueous extract of *Aloe camperi* for the delivery of ciprofloxacin, thereby enhancing its efficacy against ciprofloxacin resistant *E.coli*.

1.7. Objectives

1.7.1. General objective

- To synthesize AgNPs using *Aloe camperi* leaf extract and evaluate the *in vitro* antibacterial effect of ciprofloxacin loaded AgNPs against ciprofloxacin resistant *E.coli.*

1.7.2. Specific objectives

- To synthesize AgNPs using *Aloe camperi* leaf extract as a reducing and stabilizing agent,
- To optimize operational factors for AgNPs synthesis,
- To investigate the drug loading and drug encapsulation efficiency of AgNPs,
- To characterize the physicochemical properties of AgNPs and AgNPs-Cip,
- To determine the *in vitro* drug release profiles of ciprofloxacin loaded AgNPs and
- To evaluate the *in vitro* effect of ciprofloxacin loaded AgNPs against ciprofloxacin resistant *E. coli* as compared with ciprofloxacin and AgNPs alone

2. EXPERIMENTAL

2.1. Materials

Aloe camperi leaves were collected from the forest in South Wollo, Ethiopia. Silver nitrate (99.97%) (LobaChemie Pvt. Ltd., India) and Müller-Hinton agar (Sisco Research Laboratories Pvt. Ltd) were kindly supplied by Ethiopia Biotechnology Institute (EBTI). Ciprofloxacin hydrochloride (98.28%) was generously donated by Cadila pharmaceutical (Ethiopia) PLC. Clinical isolates of ciprofloxacin resistant *Escherichia coli* was obtained from microbial stock cultures, Microbiology and Parasitology Laboratory, College of Health Sciences, Addis Ababa University. Chloroform AR (Reagent Chemical Services Ltd., UK), sulphuric acid (98%, LobaChemie Pvt. Ltd., India), hydrochloric acid (35.4%, LobaChemie Pvt. Ltd., India), potassium iodide (99-100.5%, LobaChemie Pvt. Ltd., India), ferric chloride (99%, LobaChemie Pvt. Ltd., India), sodium carbonate (Sigma chemical company, USA), Iodine (Reagent Chemical Services Ltd., UK), gelatin powder (Blulux Laboratories Ltd., India), sodium citrate (99%, UNI-CHEM chemical reagent), copper sulphate (98.5%, Banbury, UK), sodium hydroxide (99.8% Norbright, China), potassium chloride (99% BDH Limited Poole, England), potassium dihydrogen orthophosphate 99% purity (TITAN BIOTECH LTD., India), dialysis sack (an average flat width of 35 mm and 12 kDa molecular weight cutoff, SIGMA-ALDRICH, USA), and universal indicators (Effective laboratory supplies, India) were used as received.

2.2. Methods

2.2.1. Aloe camperi leaves collection and extract preparation

Fresh leaves of Aloe camperi were collected from Harego (located at 11^{o} 10' N and 39^{o} 65' E), 3.01 Km southeast of Dessie, South Wollo, Ethiopia. The species was authenticated by the department of plant biology and biodiversity management of Addis Ababa University, Ethiopia.

Aqueous extraction of *Aloe camperi* leaf was conducted according to the method described by Tippayawat and colleagues (Tippayawat *et al.*, 2016). Briefly, the leaves were washed with tap water and then rinsed with distilled water twice to remove any dirt materials. Both sides of the edges of the leaves were removed and the rest part was cut in to small pieces (with average dimensions of 6 mm by 6 mm) with knife. Then, 50 g of the chopped leaves was heated in 50 mL of distilled water for 20 minutes at 100 ^{o}C by using a hot plate. After

boiling, it was allowed to be cooled at room temperature (25 ^{o} C). The cold extract was filtered with Whatman NO.1 filter paper. The filtrate was stored at 4 ^{o} C for the proceeding AgNPs synthesis.

2.2.2. Preliminary phytochemical screening of aqueous extract of Aloe camperi

Preliminary phytochemical screening was carried out to determine the presence of common metabolites in the aqueous extract with standard guidelines, as follows:

2.2.2.1. Screening for phenols

Ferric chloride test was employed for screening phenolic compounds as described by (Emasushan and Britto, 2018) in which 2 mL of extract was treated with 3 drops of 5 % ferric chloride solution to check the formation of bluish-black color which indicates the presence of phenol.

2.2.2.2. Screening for saponins

Foam test was applied for saponins screening in which 2 mL of extract was diluted with 10 mL of distilled water and warmed gently and was shaken for 5 minutes to check the presence of persistent foaming for 60 minutes which indicates the presence of saponin (Emasushan and Britto, 2018).

2.2.2.3. Screening for flavonoids

Alkaline reagent test was utilized for screening of flavonoids in the extract through which 2 mL of 2.0 % NaOH solution was mixed with 2 ml of aqueous plant extract to check the formation of concentrated yellow color which indicate the presence of flavonoid (Gul *et al.*, 2017).

2.2.2.4. Screening for alkaloids

Wagner's test was employed for screening alkaloids by treating 2 mL of extract with 5 drops of Wagner's reagent to check the formation of reddish brown precipitate which indicates the presence of alkaloid (Emasushan and Britto, 2018).

2.2.2.5. Screening for tannins

Gelatin test was utilized for screening of tannins in the aqueous extracts through which 1% solution of gelatin containing 10 % sodium chloride was added in to 5 mL of plant extract to check the formation of any precipitation which indicates the presence of tannin (ElKhatim *et al.*, 2019).

2.2.2.6. Screening for proteins

Biuret test was utilized for screening proteins compounds in aqueous extract. Briefly, 2 mL of extract was treated with 2 mL of 5 % NaOH and 2 mL of 1 % $CuSO_4$ solutions to check the formation of violet or purple coloration which indicates the presence of protein (Emasushan and Britto, 2018).

2.2.2.7. Screening for carbohydrates

Benedict's test was applied for screening of reducing sugar. Equal volume (0.5 mL) of extract and Benedict's solution were mixed. The mixture was heated in boiling water bath for 2 minutes to check the formation of orange red precipitate which indicates the presence of reducing sugar (Banu and Cathrine, 2015).

2.2.2.8. Screening for steroids

Salkowski's test was employed for screening of steroid in the aqueous extract. Briefly, 2 mL of extract was treated with 2 mL of chloroform in the test tube. Then, 2 m L of concentrated H_2SO_4 was added gently on the internal side of the test tube to check the formation of red chloroform layer and greenish yellow fluorescence acid layer which indicates the presence of steroid(Gul et al., 2017).

2.2.2.9. Screening for terpenoids

Salkowski's test was also employed for screening of terpenoids in which 2 mL of chloroform and 1 mL of concentrated H_2SO_4 was added to 1 mL of extract to check the formation of reddish brown color which indicates the presence of terpenoids (Emasushan and Britto, 2018).

2.2.3. Optimization of factors affecting AgNPs synthesis

For the biosynthesis of AgNPs, Song and Kim, (2009) method was adopted. Aqueous extract was poured into Erlenmeyer flask which containing aqueous solution of $AgNO_3$. The reaction mixture was kept under stirring at 500 rpm. Then the mixture was left to be cooled at room temperature overnight. The cold suspension was centrifuged at 10,000 rpm for 20 minutes for separation with centrifuge (Beckman Coulter Allegra 64R, USA). The supernatant was discarded and the solid part was re-dispersed in distilled water and re-centrifuged three times to remove free organic residue. Then the solid part was transferred into petri dish and dried at 60 ^{o}C for six hours using air dry oven.

Factors which influence the synthesis, including silver ion concentration, volume ratio of reactant, temperature of reaction, pH of the medium and reaction time were controlled by varying one parameter at a time to determine the optimum condition for the synthesis of smaller size nanoparticles with a narrow size distribution.

To determine the optimal precursor concentration for the current study, various concentrations of $AgNO_3$ were utilized, including: 0.5, 1.0, 2.0, 4.0, 8.0, 16, 18 and 32 mM while the other factors were kept constant. Similarly, the influence of percentage volume of extract, the effect temperature, pH and time of the reaction were also evaluated by varying the volume of extract (2.5, 5, 10, 20, 40, 80 and 160 %), the reaction temperature (25, 50, 75 and100 ^{o} C), pH of the reaction medium (5.0, 6.0, 8.0, 10 and 12) and reaction time (0.5, 1, 2 and 3.0 h), respectively.

The effects of operational factors on the synthesis of AgNPs were evaluated through visual observations, including color change (time taken to depict a color change and intensity of color) and precipitate formation. Furthermore, qualitative UV-visible absorbance peak analysis, including the position of the peak, the intensity of the peak and the width of the peak, was performed with Spectrophotometer carry 60, Agilent Technologies by scanning in the wave length range of 300 nm to 600 nm.

2.2.4. Synthesis of AgNPs at optimized condition

Forty mL of aqueous extract was poured into Erlenmeyer flask which contained 160 mL of 16 mM of aqueous $AgNO_3$ solution. The reaction mixture was kept at 75 ^{o} C, at pH-12 of reaction medium under stirring at 500 rpm for 2 hours. Then the mixture was left to be cooled at room temperature overnight. The cold suspension was centrifuged at 10,000 rpm for 20 minutes for separation with centrifuge (Beckman Coulter Allegra 64R, USA). The supernatant was discarded and the solid part was re-dispersed in distilled water and re-centrifuged three times to remove free organic residue. Then the solid part was transferred into petri dish and dried at 60 ^{o} C for six hours using air dry oven. Visual observations and qualitative UV-Visible analysis were employed to evaluate the synthesis.

2.2.5. Ciprofloxacin loading on AgNPs

Ciprofloxacin loading on the surface of AgNPs was done according to the method described by Lopez-Carrizales *et al*., (2018). It was commenced with the preparation of biosynthesized AgNPs suspension and ciprofloxacin stock solution using distilled water. Briefly, 150 mL stoke suspension of AgNPs with a concentration of 128µg/mL was prepared in a 200 mL of

beaker. An equal volume (150 mL) and concentration (128μg/mL) of ciprofloxacin hydrochloride stock solution was prepared in another beaker. Then, 100 mL was taken from each stock solution and poured into a 250 mL of Erlenmeyer flask, covered with aluminum foil and incubated at room temperature, under constant stirring at 180 rpm for 12 hours. After the incubation period, it was subjected to centrifugation at 10, 000 rpm for 20 minutes by using a centrifuge (Beckman Coulter Allegra 64R, USA). The supernatant was collected in clean beaker. The residue was re-dispersed with distilled water and re-centrifuged three times to remove free ciprofloxacin.

The influences of incubation time and drug concentration on the encapsulation efficiency and drug loaded content of AgNPs were investigated by incorporating more incubation times (6, 24, 48 and 72 h) and drug's concentrations (64, 256, 384, 512 μg/ml). Every measurement was performed in trice and the average values were recorded. To demonstrate their impact, the percentage drug loading profiles of AgNPs as a function of time and ciprofloxacin concentration were plotted.

2.2.5.1. Determination of encapsulation efficiency and drug loading capacity

The encapsulation efficiency and the percentage drug loaded content were evaluated by calculating free ciprofloxacin in the total supernatant from a linear equation and substituting the corresponding values in simple mathematical equations (Eq. 1 and Eq. 2).

Briefly, after determining the λ-max, the linear calibration curve was constructed using six different concentrations (1, 2, 3, 4, 5 and 6 μg/mL) of standard ciprofloxacin hydrochloride with UV/Vis spectrophotometer (Spectrofluorimeter CM 2203, Republic of Belarus) at 275 nm. All readings were taken in triplicate and the average values were presented. The linear equation and linear fit were determined with Originpro 8.5 software package. The absorbance of unloaded ciprofloxacin was recorded in the range of the linear curve and the corresponding unknown concentrations were calculated from the equation. Then, the percentage encapsulation efficiency of AgNPs and percentage drug loading content were determined as described by Shaker and colleagues in the following equations (Shaker and Shaaban, 2017).

Encapsulation efficiency (%)

$$= \frac{\text{(total ciprofloxacin – ciprofloxacin in supernatant)}}{\text{total ciprofloxacin}} \times 100\ \% \ldots \text{Eq.1}$$

Drug loading (%)

$$= \frac{\text{(total ciprofloxacin – ciprofloxacin in supernatant)}}{\text{(amount of AgNPs + amount of loaded ciprofloxacin)}} \times 100\ \% \ldots \text{Eq.2}$$

The probable wastage of ciprofloxacin through adsorption in the inner surface of centrifugation tube was ruled out by centrifuging 45 mL (volume of centrifugation tube) of 1 mg/mL of ciprofloxacin hydrochloride at 10, 000 rpm for 20 minutes and measuring the concentrations before and after centrifugation which were found to be the same.

2.2.6. Characterizations of AgNPs and AgNPs-Cip

2.2.6.1. UV-visible (UV-Vis) spectroscopy

The optical property of synthesized AgNPs and AgNPs-Cip was qualitatively analysed with UV/Vis. (Spectrophotometer carry 60, Agilent Technologies), scanning from 200.00 to 800.00 nm with scanning rate of 24000.000 (nm/min). The absorbance (a.u) versus wave length (nm) spectrum was plotted for every plasmon peak analysis.

2.2.6.2. Fourier-transform infrared (FTIR)

The FTIR spectrophotometer (Perkin Elmer, spectrum 65), scanned in the region 4000-400 cm^{-1} was employed to identify the possible functional groups of phytochemicals which were responsible for the reduction and stabilization processes of AgNPs synthesis. It was also utilized to detect the functional groups of ciprofloxacin associated with surface functionalization.

2.2.6.3. Dynamic light scattering (DLS)

The size and polydispersity index (PDI) of the synthesized AgNPs and the AgNPs-Cip were estimated with 90 plus particle size analyzer (Brookhaven Instruments Corporation, USA) with a fixed wavelength of 659 nm at 90 ° detection angle. The suspension was prepared in deionized water. It was sonicated for 30 minutes before analyzing to avoid aggregation (Bhaumik *et al.*, 2015). The sample was passed through micro filter (0.22 mm of pore size) to discard dusts and macro particles before loaded into the cuvette. The measurements were repeated by diluting the sample until approximately constant values were recorded while the

average count rate and base line index were maintained in optimal working condition from 50- to 300 Kcps and above 7, respectively.

2.2.6.4. Scanning electro-microscope (SEM)

The surface morphology of biosynthesized AgNPs were examined with scanning electron microscope (TESCAN VEGA3 SBU, Brno, Czech Republic).

2.2.6.5. X-ray diffraction (XRD)

The crystallinity of the biosynthesized AgNPs was confirmed by X-ray diffractometer (XRD-7000 x-ray diffractometer, Shimadzu Corporation, Japan), working with a voltage of 40 kV and current of 30 mA. A monochromatic beam of cupper radiation (λ = 0.15406 nm) was utilized to examine the biosynthesized AgNPs sample through scanning at 2Θ over the range of 10 to 80 ^{o}. The nature of crystallinity and the crystalline structure were determined with X'Pert HighScore plus 2.1 software package (Malvern Panalytical). The average size of crystallite was also estimated by using Debye-Scherrer's equation (Ajitha *et al.*, 2014).

$$D = \frac{K\lambda}{\beta \cos \Theta} \quad \ldots \text{Eq.3}$$

(where D denotes the crystallite size, K the Scherrer constant (0.9), λ wavelength of Cu Kα radiation, β full-width at half-maximum of diffraction line and Θ half diffraction angle)

2.2.6.6. Differential scanning calorimeter - thermogravimetric (DSC-TGA)

The thermal profile of AgNPs was examined with DSC-TGA (SDT Q600 V20.9 Build 20, Universal V4.5A TA instruments). After sample was loaded on the pan and measured the net weight (20.01mg), it was scanned across temperature ranges from 0 to 700 ^{o} C. As output, simultaneous DSC-TGA thermograph were plotted to demonstrate the thermal properties of biosynthesized AgNPs.

2.2.7. *In vitro* drug release studies

The calibration curves of standard ciprofloxacin hydrochloride at four different pH media (pH of 1.2, 6.0, 6.8, and 7.4) were constructed after determining their corresponding λ-max of 276, 276, 270 and 268 nm, respectively. Then, six different concentrations of ciprofloxacin hydrochloride were prepared with each pH medium, including 2.0, 4.0, 6.0, 8.0, 10 and 12 mg/mL. The corresponded absorbance was measured with UV/Vis spectrophotometer (Spectrofluorimeter CM 2203, Republic of Belarus). All readings were taken in triplicate and

the average values were presented. The linear equation and linear fit were determined with Originpro 8.5 software package.

The *in vitro* release profile of ciprofloxacin from the surface of AgNPs was investigated by employing the dialysis sac method. The procedures were adopted from Shaker and Shaaban, (2017). Briefly, each piece of dialysis sacks (with 3.5 cm width and MWCO of 12 kDa) was soaked into four different specific pH media (pH of 1.2, 6.0, 6.8, and 7.4) overnight. Three mg/mL solution of the loaded particle was prepared in each of the aforementioned pH medium which was kept into four different 50 mL beakers. Then, 5 mL was pipetted out from one beaker and dropped into a piece of an overnight soaked dialysis bag of which the one opening-end was already tightly tided. After the whole volume was transferred, the other end of the dialysis bag was tourniqueted with thin rope and immersed into a 100 mL of conical flask containing 50 mL of the corresponding pH medium. The same procedures were followed for the other three beakers. Then, each flask were covered with aluminum foil and maintained on the Shaker (Heidolph Unimax 1010, Heidolph instruments, Germany) at 100 rpm. At every hour for the first 5 hours followed by every 12 hours interval, 5 mL of the sample was taken from the releasing medium for spectroscopic analysis. The sink condition was maintained by replacing with an equal volume of the same pH fresh medium after each sample collection. The absorbance of each sample was recorded using UV-visible spectroscopy at pre-determined λ-max for each corresponding pH medium. Every measurement was taken in trice and the average value was presented. The concentration of released ciprofloxacin was calculated from the calibration curve which had already been constructed. Then, the percentage cumulative ciprofloxacin release was determined by the standard formula of $[Drug]_t/[Drug]_{total}$, where $[Drug]_t$ denoted to the amount of drug released at time 't' and $[Drug]_{total}$ referred to the total amount of loaded drug. The graphs of percentage cumulative ciprofloxacin release at each pH medium versus time were plotted using Originpro 8.5 software package.

2.2.8. *In vitro* antimicrobial susceptibility test

Before *in vitro* antimicrobial susceptibility test (AST), the isolated resistant strain was confirmed by standard ciprofloxacin disc method.

The *in vitro* susceptibility test was conducted by employing disk diffusion test on Müller-Hinton agar (MHA) according to Clinical and Laboratory Standards Institute (CLSI) guideline (CLSI, 2020). Briefly, 39 g of dehydrated MHA was suspended into 1 L of distilled

water, under thoroughly mixing. After completely dissolving the components, it was subjected to autoclave at 121 ° C for 15 minutes. Then 25 mL of the solution was dispensed and uniformly distributed on the surface of each plate with sterile swab. The plates were allowed to solidify at room temperature, and then stored at 4 ° C.

The free cellulose paper disc with 6 mm diameter was prepared from Whatman No 3 filter paper using a paper puncher and then autoclaved (Vineetha *et al.*, 2015). The stock solutions of ciprofloxacin hydrochloride, AgNPs-Cip and AgNPs were prepared with their corresponded concentration of 1, 1.82 and 0.82 mg/mL, respectively. Then, 5 mL was taken from each stock solution with micropipette and impregnated in paper discs. After being dried in a clean incubator at 37 ° C for 4 hours, discs were dispensed on the surface of inoculated agar plate and labeled correctly. The assay was performed in triplicate and the mean values were reported.

After 18 hours of incubation, the complete of inhibition zone (mm) was measured by taking the mean diameter with ruler. The interpretation was determined according to CLSI guideline breaking points (CLSI, 2020) and the fold increase area was determined by the equation as described by (Birla *et al.*, 2009).

$$\text{The fold area increase} = \frac{B^2 - A^2}{A^2}$$

(Where A and B denoted inhibition zones by free ciprofloxacin and the loaded particles)

3. RESULTS AND DISCUSSION

3.1. Plant extract preparation and phytochemicals screening

Light yellow aqueous plant extract, as displayed in **Error! Reference source not found.**A was obtained through the extraction method utilized.

The results of preliminary phytochemical screening are summarized in Table 1. It provided quick and qualitative information about the existing group of metabolites in the aqueous extract. As indicated in the table, the aqueous extract comprised phenols, saponins, flavonoids, tannins, proteins and carbohydrates. Most of these biomolecules were also reported by the previous phytochemical screening of water extract of *Aloe camperi.* However, the report included other phytochemicals which were not detected in the current study (Demoz *et al*., 2015). The difference may be due to the variation in extraction procedures.

Due to the diverse nature of phytochemicals in plant extract, it is cumbersome to isolate the specific biomolecules responsible for the reduction and stabilization of metal nanoparticles. Even though, specific biosynthesis mechanism has not fully understood yet, phytocomponents including polyphenols (flavonoids, phenolic acid and tannins), saponins, proteins and carbohydrate considered as a potential reducing and stabilizing agents for metal nanoparticles synthesis (Ovais *et al.*, 2018, Segura *et al.*, 2020, Kim *et al.*, 2016). Their hydroxyl, carbonyl, alkane and alkene functional groups had the ability to reduce and stabilize metal nanoparticles (Vaseghi *et al.*, 2018) which were also detected during FTIR analysis of this study.

Table 1: Preliminary phytochemical screening of aqueous leaf extract of *Aloe camperi*

Screened metabolite	Type of test Performed	Expected changes	Result
Phenols	Ferric chloride test	Bluish-black color	+
Saponins	Foam test	Persistent foaming	+
Flavonoids	Alkaline reagent test	Concentrated yellow color	+
Alkaloids	Wagner's test	Reddish brown precipitate	-
Tannins	Gelatin test	Precipitation	+
Protein	Biuret Test	Violet or purple color	+
Carbohydrate	Benedict's test	Orange red precipitate	+
Steroid	Salkowski's Test	Red chloroform and greenish yellow acid layer	-
Terpenoids	Salkowski's Test	Reddish brown color	-

3.2. Optimization of factors affecting AgNPs synthesis

3.2.1. Visual observations

During visual observations, the reaction mixture underwent a color changes from almost colorless to a stable dark brown within 2 hours. The reaction rate was found to be dependent on operational variables. As the concentration of $AgNO_3$ increased from 1 mM to 16 mM, the reaction rate became faster and faster. This was observed from the rate of color changes which took only 3 minutes for sample that contained 16 mM of $AgNO_3$ as compared to 15 minutes for sample contained 1 mM of $AgNO_3$. A clear precipitation was observed in the samples contained $AgNO_3$ with concentration of 16 mM and more. Similar observation was reported by Ulaeto and colleagues in their study on biogenic AgNPs extract from Neem extract (Ulaeto *et al*., 2019).

As the result of change in volume of extract revealed, all test samples except those containing 2.5 % (V/V) of extract, took only 3 minutes to undergo color changes. The test sample contained 2.5 % (V/V) of *Aloe camperi* extract remained unchanged throughout the reaction time. Furthermore, there was no solid mass after cooling and centrifugation. This was due to lack of adequate metabolites which are crucial for the synthesis and stabilization of AgNPs.

The rate of color change was also temperature dependent. An immediate color change was observed at 75 ^{o} C and 100 ^{o} C while it took 11 minutes at 25 ^{o} C. This may be due to the faster kinetics of the molecules at high temperature, facilitates rapid intermolecular collusions which leads to facile reaction.

As revealed from the Figure 7, an immediate color change from light yellow to brown was observed in alkaline media. However, it remained yellow-orange in acidic medium (pH-3) throughout the reaction time. Hence, in acidic medium the biosynthesis of AgNPs with *Aloe camperi* aqueous extract could not be achieved. This may be due to the acidic pH compromised the ionization of phytochemicals which were responsible for reduction and capping in synthesis. This was also confirmed through UV-visible analysis as displayed in Figure 9.

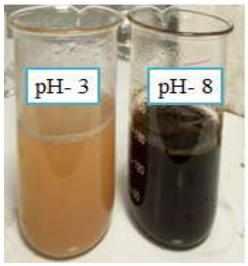

Figure 7: A comparative photographic presentation on the visual appearances of the mixture of $AgNO_3$ and *Aloe camperi* extract at acidic (pH-3) and basic (pH-8) reaction media.

A stable dark brown suspension was attained within 2 hours of reaction. This implies 2 hours is sufficient to complete the reaction. The spectroscopic analysis (Figure 12) was also consolidated this suggestion.

3.2.2. Spectroscopic analysis

Furthermore, the formation of AgNPs was determined with UV-Visible spectroscopic analysis. As surface plasmon resonance (SPR) is an outstanding optical property of metallic nanoparticles (Vila *et al*., 2016). Hence, the distinct characteristic plasmon peak appeared

around 420 nm in the UV-Visible spectra (Figure 8 to 13) confirmed the synthesis of AgNPs. This was corroborated by many previous scientific reports (Pataki *et al.*, 2020, Muggeo *et al.*, 2020, Hemlata *et al.*, 2020).

As the results illustrated, the UV-visible analysis of the current study was in contrast to Song and Kim's work that reported the decrement of average particle size with the increment of $AgNO_3$ concentration. These paradoxical results may be raised from the uniqueness of each plant extract-mediated biosynthesis of metal nanoparticles. In the present study, the optical density was found to be increased as the concentration increased from 0.5 mM (Abs = 0.076) to 16 mM (Abs = 1.953) as shown in Figure 8 below. Beer Lambert law stated that the peak height of the surface plasmon band is proportional to the concentration which in this scenario signifies the production of more nanoparticles (Nogueira *et al.*, 2014, Roldán *et al.*, 2008). Similar result was reported by Huang and colleagues who studied the effect of precursor concentration in biosynthesis of AgNPs with *Cacumen platycladi* extract (Huang *et al.*, 2011).

Moreover, a bathochromic shift (to λ-max at 430 nm) was observed with higher concentration of $AgNO_3$ (18 mM and 32 mM). This may be due to the aggregation of the nanoparticles that leads to higher particle size. According to the Mei theory smaller nanoparticles absorbs at shorter wave length and larger nanoparticles absorbs at longer wave length in the UV-visible spectrum (Ulaeto *et al.*, 2019). This relationship also corroborated by several previous studies on the optical properties of AgNPs (Ghiuță *et al.*, 2018, Agnihotri *et al.*, 2014). Therefore, 16 mM of precursor concentration which provided higher number of nanoparticles with smaller size was qualitatively determined for the proceeding nanoparticles synthesis.

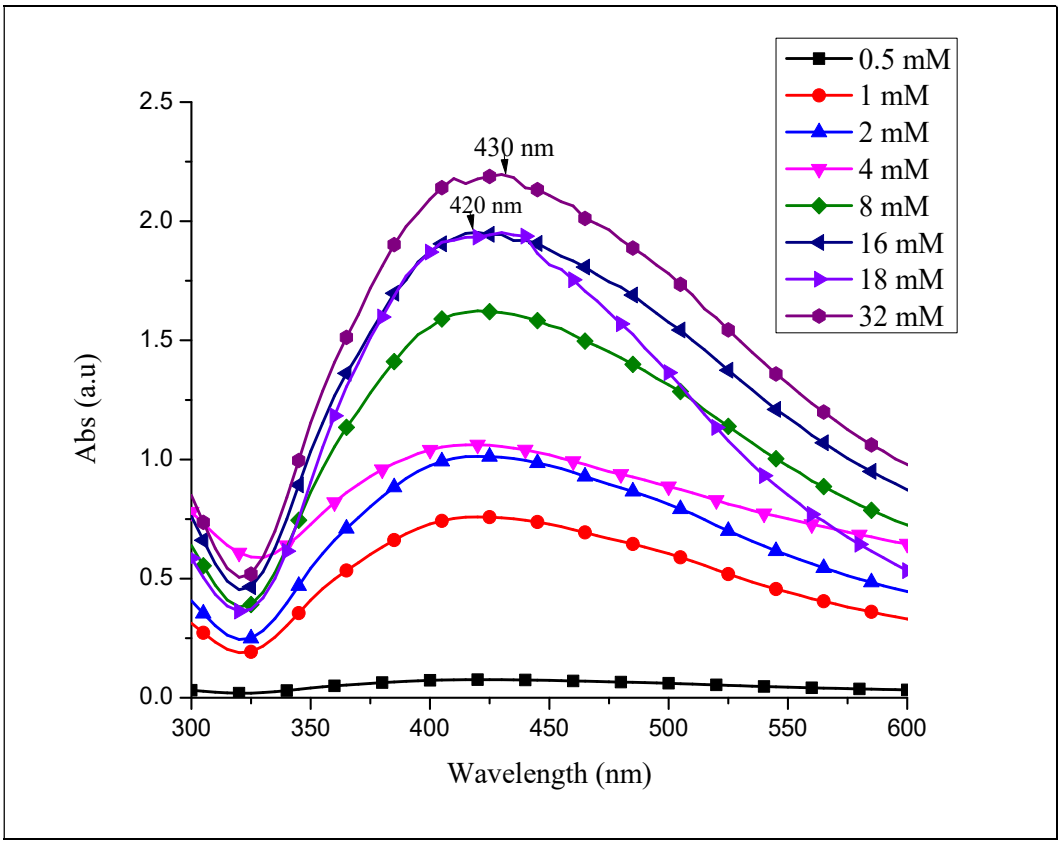

Figure 8: UV-Visible absorption spectra of biogenic AgNPs over different concentration of $AgNO_3$

The characteristics of plasmon peaks were also varied with the percentage of plant extract as displayed in the UV-visible spectra (Figure 9). There was no distinctive peak observed for a sample that contained 2.5 % of extract. This is due to the insufficient reducing and stabilizing metabolites. As the percentage of extract increased from 10 % to 20 %, the plasmon peak was shifted to the shorter wave length (from 420 nm to 415 nm). But when the volume of extract was further increased to 40 % and 80 %, the plasmon peak showed a bathochromic shift to 425 nm and 460 nm respectively. This demonstrated that excess amount of plant metabolites led to the aggregation of synthesized AgNPs. Song and Kim suggested two possible reasons for particle size growth under excess reducing agent (1) interactions between capping biomolecules and (2) secondary reduction processes on the surface of the nuclei (Song and Kim, 2009). Furthermore, the narrowest peak band was observed with 20 % (v/v) extract. Hence, 20 % (v/v) of aqueous *Aloe camperi* extract was determined as optimal amount for the proceeding parameter optimizations.

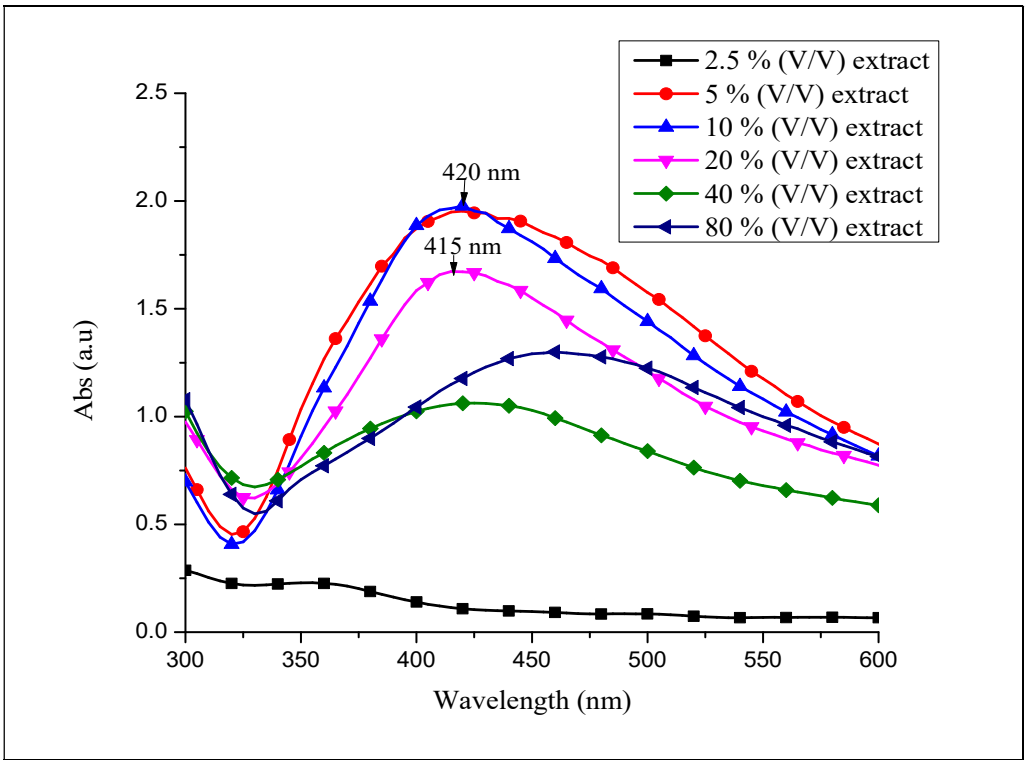

Figure 9: UV-visible absorbance spectra of biosynthesized AgNPs over different volume of extract

As exhibited from Figure 10, the reaction temperature influenced both the position and intensity of plasmon peak during UV-visible analysis. At lower temperature, the widest band with the least absorbance at longer wavelength (Abs = 0.88, λ-max = 455) was recorded. While the temperature was increased from 50 ^{o} C to 75 ^{o} C, the intensity of the peak was increased without any shift (at 415 nm). However, further increasing the temperature did not result change in peak height. From this qualitative UV-visible analysis we suggested that as the temperature increased, the size of nanoparticles decreased leading to more nanoparticles production. This may be due to the faster kinetics of the molecules at high temperature, facilitates rapid intermolecular collusions in which silver ion consumed faster in nucleation, leaving less probability to be involved in particles aggregation. Nevertheless, further increase in temperature was resulted decrease in peak intensity. Since, some metabolites may be degraded at high temperature (Huang *et al*., 2011, Jain and Mehata, 2017, Bhaumik *et al*., 2015). Therefore, 75 ^{o} C of the reaction temperature which provided the higher optical density at shorter wavelength was chosen as optimal value for the current study.

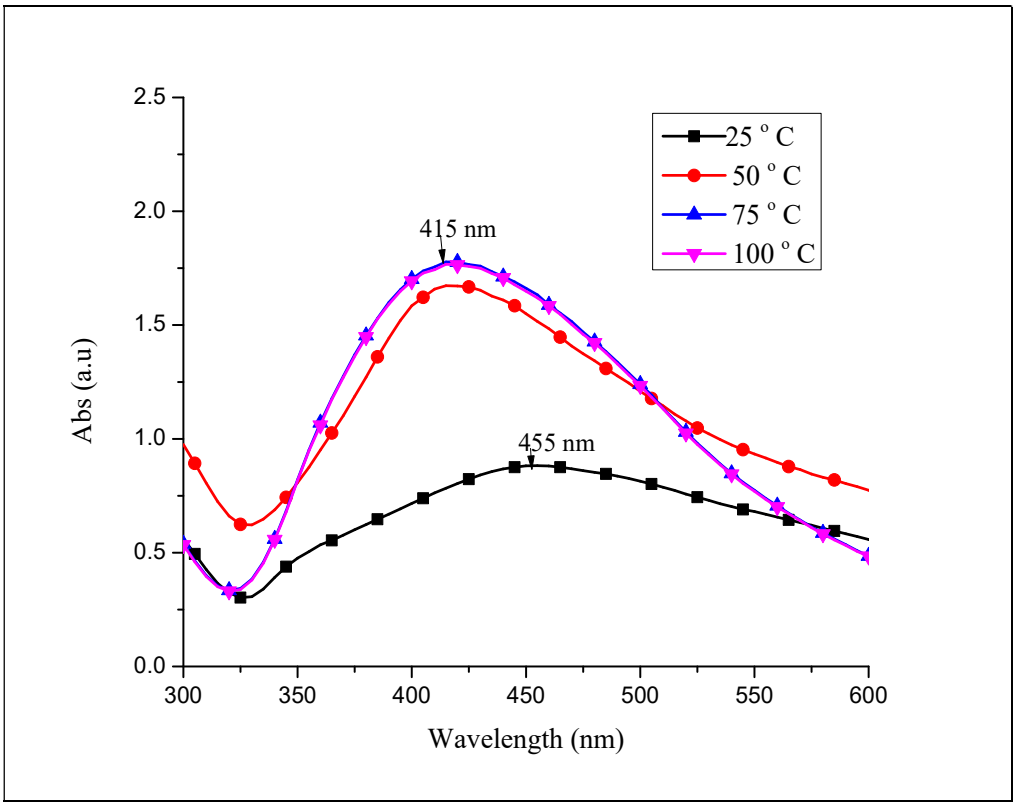

Figure 10: UV-Visible absorbance spectra of biosynthesized AgNPs over range of reaction temperature

As the pH of the reaction media increased from 6 to 12, the absorbance peak was slightly increased with blue shift (to 410 nm) as depicted in Figure 11. Furthermore, there was no distinctive absorbance peak appeared at acidic condition (pH-3). This result is in good agreement with many scientific reports in the area (Marciniak *et al.*, 2020, Baghizadeh *et al.*, 2015, Logaranjan *et al.*, 2016, Bhaumik *et al.*, 2015). However, other researchers like Jain and Mehata who synthesized silver nanoparticles using Tulsi extract, reported a peak shift to the longer wavelength as pH increase (Jain and Mehata, 2017).

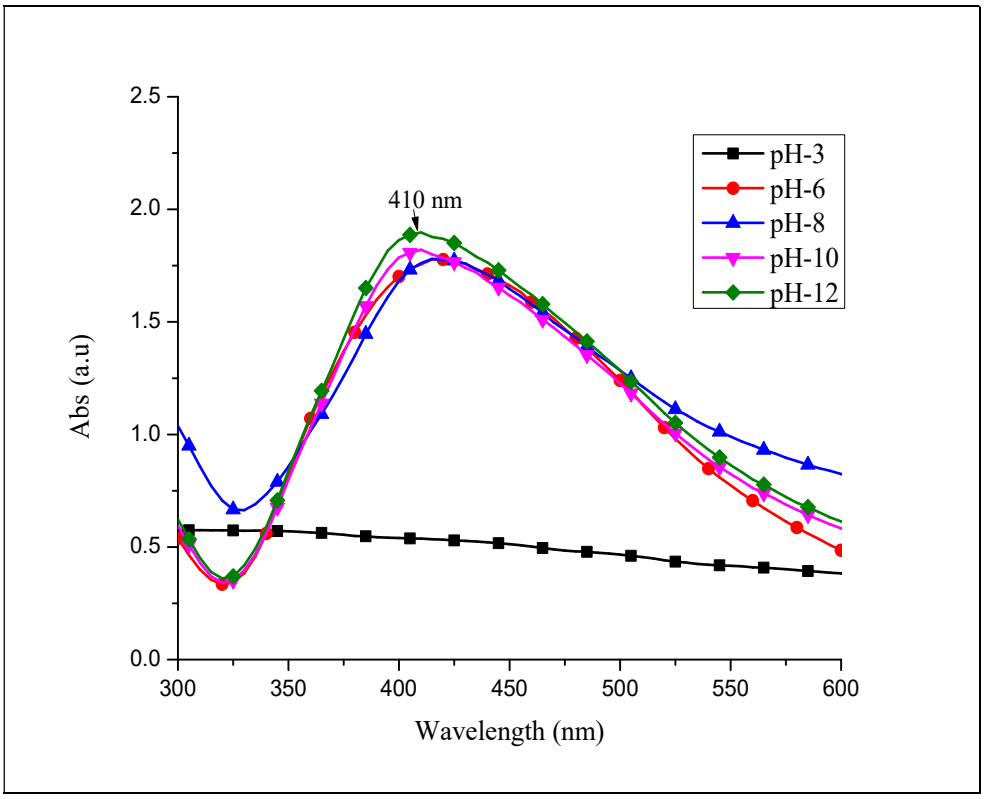

Figure 11: UV-Visible absorbance spectra of biosynthesized AgNPs over pH range of reaction medium

As shown in Figure 12, without any peak shift, the optical density was increased for the first 2 hours then stabilized due to the completion of the reaction. Hence, 2 hours was taken as sufficient reaction time for the final nanoparticles synthesis. Therefore, based on our optimization study we have determined that a combination of 16 mM of $AgNO_3$ concentration, 20 % of extract, 75 ^{o} C of reaction temperature, pH-12 of the reaction medium and 2 hours of reaction time as optimal condition for the final synthesis of the AgNPs.

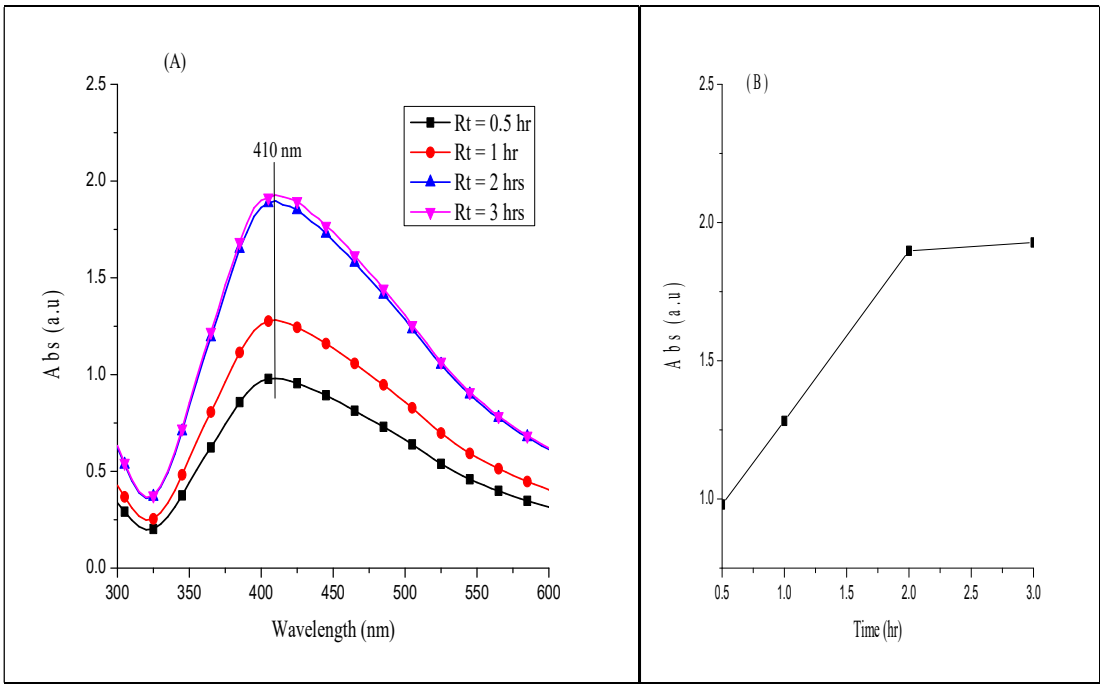

Figure 12: UV-Visible absorbance spectra of biosynthesized AgNPs over different reaction time (A) and the graph of absorbance at 410 nm versus reaction time (B)

3.3.Synthesis of AgNPs at optimized condition

Visual observation and UV-visible spectroscopic analysis confirmed a successful synthesis of AgNPs at optimum reaction condition. The observed color change and UV- visible spectrum are clearly illustrated in Figure 13.

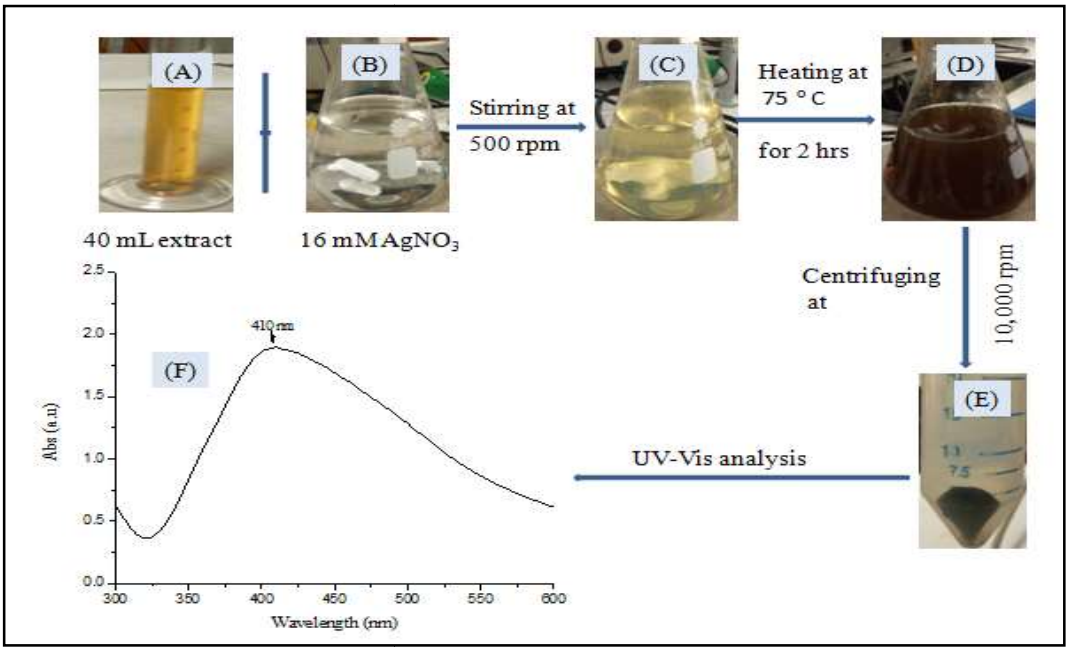

Figure 13: Photographic illustration of the observed color change during AgNPs synthesis at optimum condition and its UV-Vis spectrum.

The alphabets (A), (B), (C) and (D) represent the aqueous plant extract, $AgNO_3$ solution, the reaction mixture at time t = 0, the observed color change within 2 hours, respectively. (E) and (F) denote solid mass of AgNPs and its UV-Vis spectrum '|' = mixing, the arrow sign indicate the direction of the processes.

3.4. Ciprofloxacin loading on AgNPs

3.4.1. Encapsulation efficiency and drug loading capacity

A calibration curve of standard ciprofloxacin hydrochloride was constructed with a linear equation and correlation coefficient of $Y = 0.1038X + 0.0199$ and $R^2 = 0.9997$; where Y, X and R^2 denoted absorbance, concentration and correlation coefficient, respectively (Appendix-1) for determining the unknown drug concentration in the supernatant.

As the results revealed, ciprofloxacin hydrochloride was successfully loaded on the synthesized AgNPs. Different literatures reported the impact of drug concentrations on the drug loading capacity of AgNPs. They also utilized different incubation time for drug loading processes (Sadat Shandiz *et al*., 2017, Prasad *et al.*, 2013). In this study, the percentage of encapsulation efficiency and loading drug content were varied from 31.34 % ± 1.5 to 60.94 %

± 0.25 and 16.58 % ± 0.2 to 57.83 % ± 0.75, respectively depending on the incubation time and drug concentration as elaborated below.

3.4.1.1. Effects of incubation time and drug concentration

The smallest amount of encapsulation efficiency and drug loading content were recorded at 6 hours incubation time. When the incubation time was extended to 12 hours these values were increased as clearly depicted in Figure 14. Nevertheless, further increase in time, did not show any significant improvement in percentage of encapsulation efficiency and drug loading content. This suggests that ciprofloxacin hydrochloride requires optimal incubation time to form a stable surface adsorption on AgNPs to achieve maximum loading. Accordingly, 12 hours was chosen as optimal incubation time for loading of ciprofloxacin hydrochloride on synthesized AgNPs.

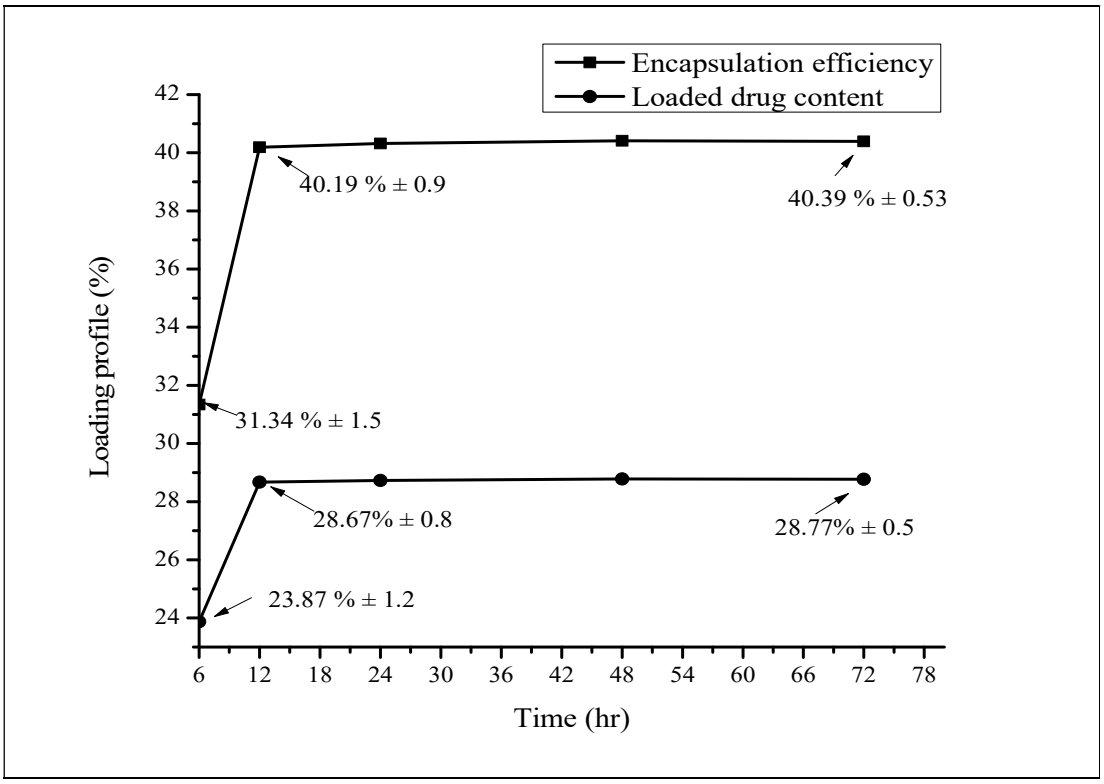

Figure 14: Graphical presentation of drug loading profiles of synthesized AgNPs as a function of incubation time

Note: Equal concentration and volume of AgNPs and ciprofloxacin hydrochloride (128 mg/mL with 100 mL) were incorporated throughout the study periods.

Drug concentration was also one of the major factors influencing the loading capacity of the nanoparticles. When concentration ratio of ciprofloxacin hydrochloride to AgNPs was increased from 1:2 to 2:1, the corresponding encapsulation efficiency and drug loading content were elevated from 39.75 % ± 0.2 to 60.94 % ± 0.25 and 16.58 % ± 0.2 to 54.93 % ± 0.2, respectively. However, further increment of drug to AgNPs ratio to 3:1 and 4:1 were resulted in sharp decrease in the encapsulation efficiency while the percentage drug loading capacity was slightly increased as shown in the graph (Figure 15). Since, the principle of drug loading on AgNPs is surface adsorption (Prasad et al., 2013, Sadat Shandiz et al., 2017), the surface can be saturated at high drug concentration. Hence, a 2:1 ratio of ciprofloxacin hydrochloride to AgNPs was taken as optimal concentration ratio for our study.

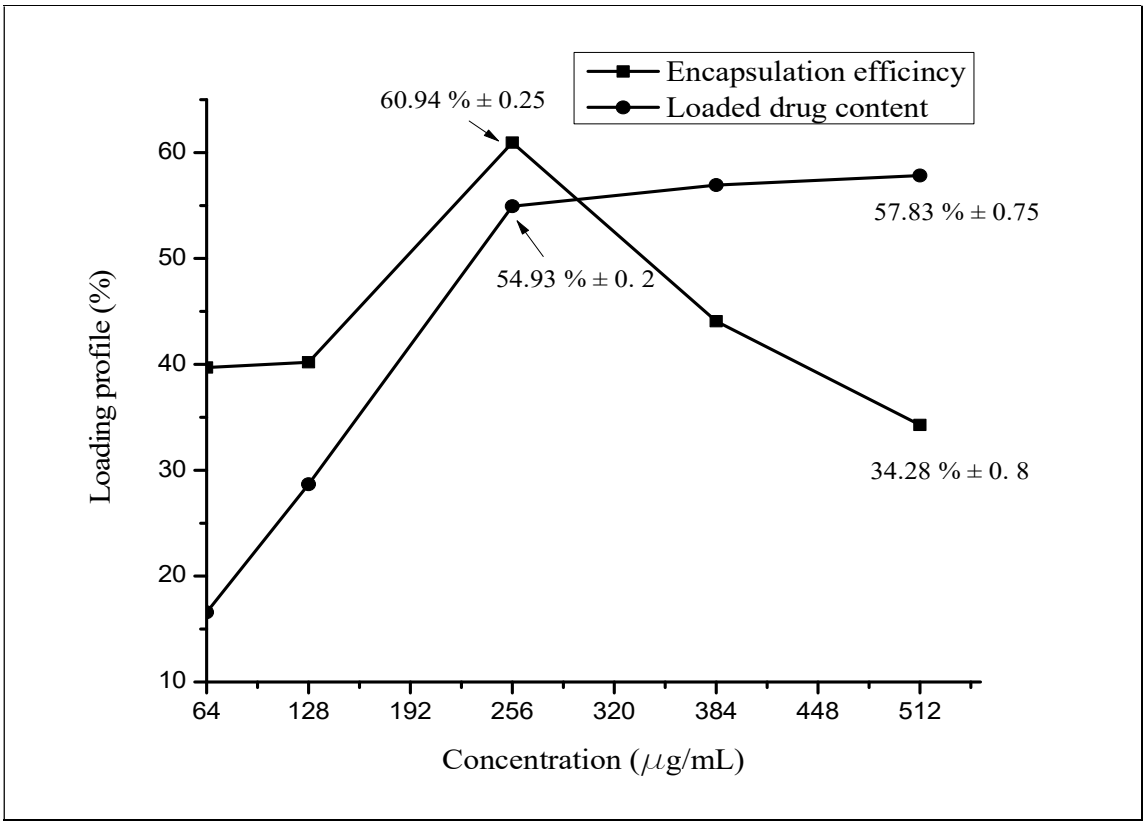

Figure 15: Graphical demonstration of drug loading profiles of synthesized AgNPs as a function of drug concentration

Note: The volume of ciprofloxacin hydrochloride (100 mL), the volume and concentration AgNPs (100 mL and 128 mg/mL) were constant throughout the study periods.

3.5. Characterizations of AgNPs and AgNPs-Cip

Precise particles characterization is a milestone in nanoparticles investigations. Since, the physicochemical properties of the nanoparticles significantly influence their intended applications. Many analytical techniques have been utilized to provide comprehensive information about the synthesized nanoparticles (Zhang *et al*., 2016, Pryshchepa *et al*., 2020).

3.5.1. UV-visible spectroscopy (UV-Vis)

According to UV-visible spectroscopic analysis a change in plasmon peak was observed after ciprofloxacin loading. As shown in Figure 16 below, the broad absorption peak was appeared with a red shift to 445 nm as compared to the free AgNPs (λ-max of 410 nm, **Error! eference source not found.**). This is attributed to the adsorption of ciprofloxacin on the surface of AgNPs which may result in elevation of the average refractive index of the surrounding environment and increasing the size of nanoparticles around the surface (Mohsen *et al.*, 2020). Furthermore, the small peak depicted around 275 nm signified the existence of ciprofloxacin on the surface of AgNPs.

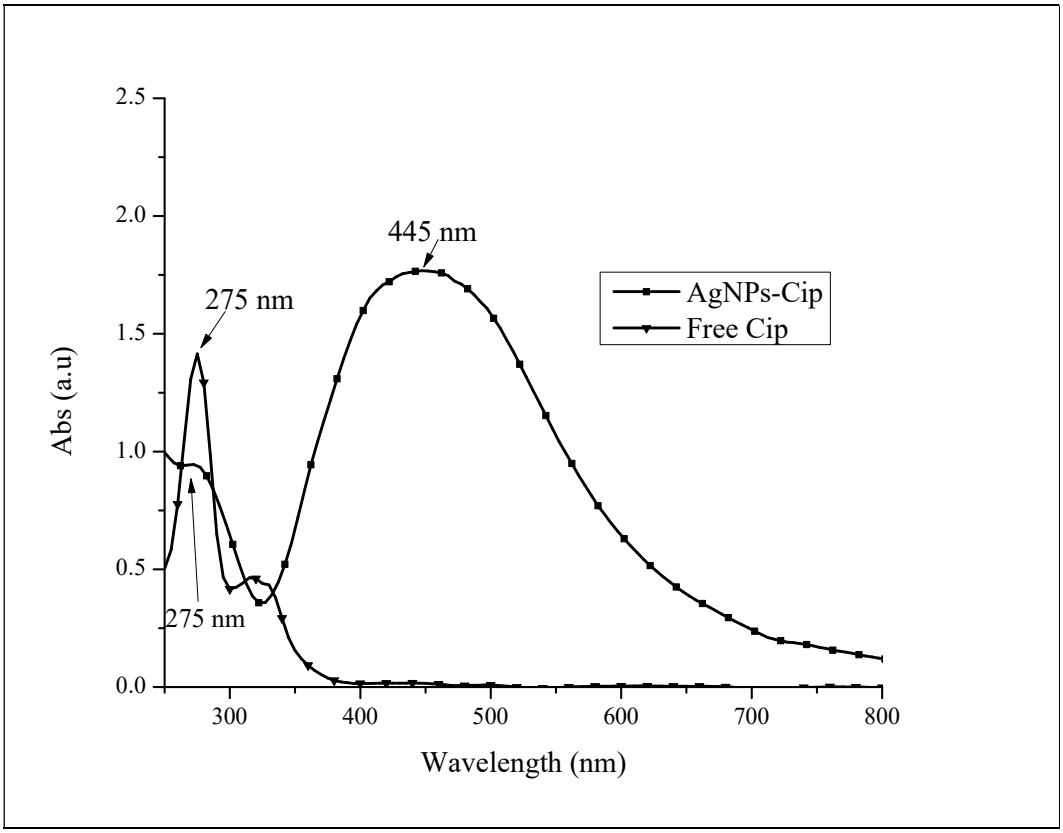

Figure 16: UV-Visible absorbance spectra of free ciprofloxacin and loaded particles

3.5.2. Fourier-transform infrared (FTIR)

The intense characteristic peaks of pure *Aloe camperi* leaf extract were appeared in the FTIR spectra as displayed in Figure 17A. Strong bands exhibited at 3325 cm^{-1} and 1634 cm^{-1} were most probably due to O-H stretching of polyphenols and aromatic C=C stretching or the presence of carbonyl group, respectively (Murei *et al.*, 2020, Jain and Mehata, 2017). Other less intense peaks depicted at 2988 cm^{-1}, 2901 cm^{-1} and 1066 cm^{-1} indicated the presence of C-H stretching's of alkene, alkane and C-O stretching of alcohol respectively (Roni *et al.*, 2013). As exhibited in the Figure 17B, most characteristics bands observed in plant extract were also appeared in the synthesized AgNPs FTIR spectrum with little shift. Similar observations were also reported by Ahmed and collogues (Ahmad *et al.*, 2016). This implies that, the hydroxyl groups of polyphenols and the carbonyl groups as well as the alkane and alkene functional groups present in aqueous plant extract were involved in the reduction of Ag^{+} to Ag^{0} and stability of the nanoparticles.

FTIR spectroscopic analyses were also performed for ciprofloxacin hydrochloride and AgNPs-Cip to detect the major responsible functional groups for adsorption. Despite the FTIR result does not provide a definitive conclusion about the mechanism of loading, it can help to suggest the probable functional groups of ciprofloxacin involved in surface interaction. As revealed from the FTIR spectrum (Figure 17C), the prominent peaks for ciprofloxacin were observed at 3379 cm^{-1}, 3085 cm^{-1}, 2929 cm^{-1}, 1709 cm^{-1}, 1625 cm^{-1}, 1385 cm^{-1}, and 1029 cm^{-1} which were assigned to O-H stretching, C-H stretching of aliphatic alkene and alkane, the C=O vibration of carboxylic group, the C=O of ketone or C=C of aromatic group, protonated amine group in the piperazine moiety and C-F vibration (Li *et al.*, 2011, Gu and Karthikeyan, 2005, Wu *et al.*, 2003, Sahoo *et al.*, 2011). After loading, the major peaks were also existed in the spectrum (Figure 17D). The broad band of O-H stretching of pure ciprofloxacin hydrochloride was shifted from 3379 cm^{-1} to 3434 cm^{-1} after loading. This result was in concordance with a previous report by Mohsen and collogues who studied the characterization of ciprofloxacin loaded AgNPs. This may be due to the –OH group of ciprofloxacin formed a hydrogen bond with phytochemicals on the surface of the AgNPs (Mohsen *et al.*, 2020). The C=O stretching vibration of carboxylic group was also detected at 1700 cm^{-1}. Most characteristic bands of the nanoparticles and ciprofloxacin were overlapped hence cannot be resolved with this technique.

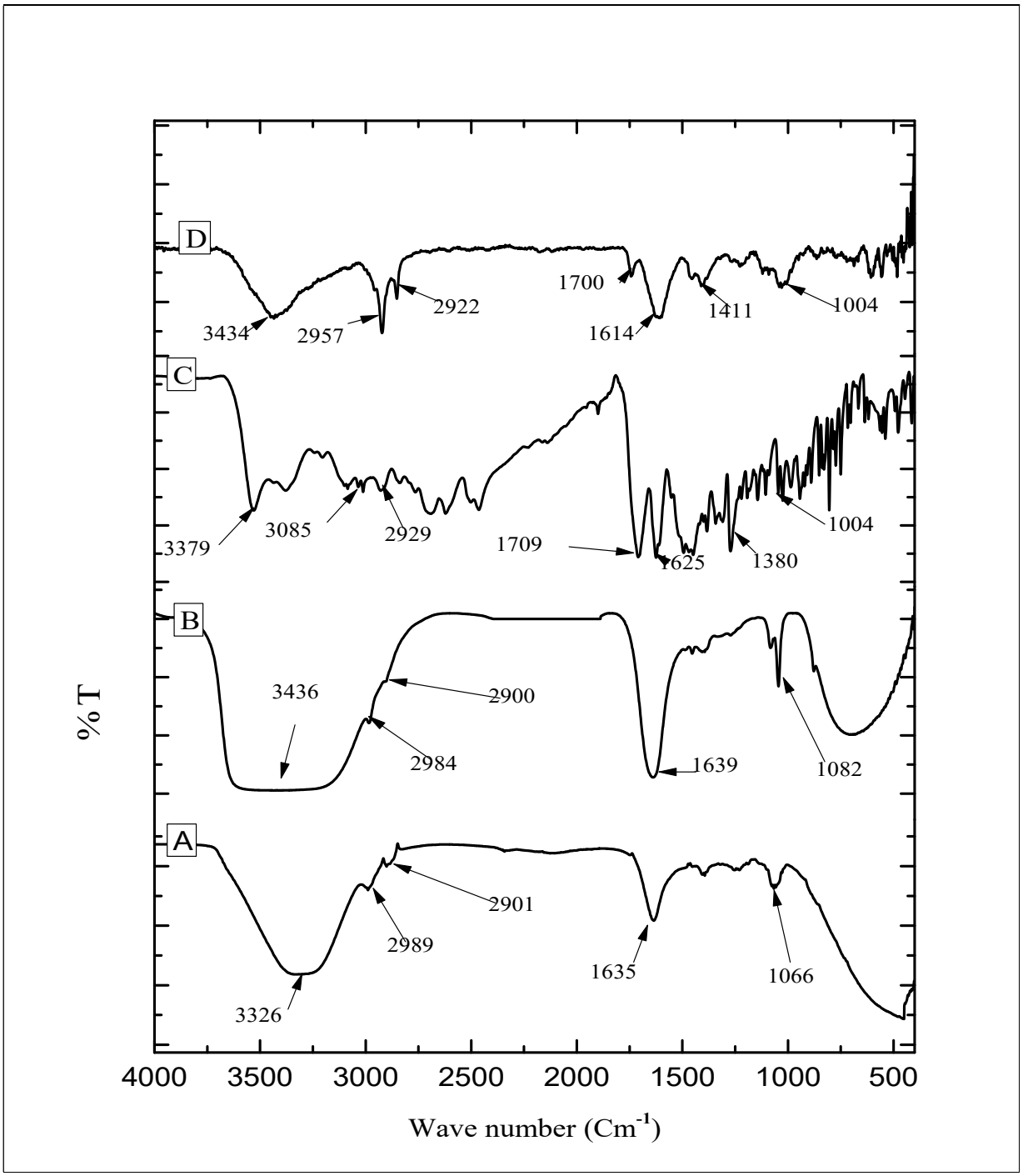

Figure 17: FTIR spectra of (A) aqueous extract of aloe camperi, (B) biosynthesized AgNPs, (C) free ciprofloxacin, (D) AgNPs-Cip

3.5.3. Dynamic light scattering (DLS)

The DLs diagrams of synthesized AgNPs and AgNPs-Cip were displayed in Figure 18A and B. As the result demonstrated, the average hydrodynamic diameter of AgNPs was 98.9 nm ± 0.3 with a polydispersity index (PDI) of 0.197 ± 0.009 As the existence of different biomolecules in the extract, the production of various sized nanoparticles was expected (Hemlata *et al*., 2020). After loading, the estimated size increased to 126 nm ± 0.4 (with PDI of 0.157 ± 0.001) due to the adsorption of ciprofloxacin on the surface of AgNPs. The DLS size estimation was higher than those recorded by SEM images and the calculated crystallite size using XRD. Since, SEM measures only the core of metallic nanoparticles. However, DLS measures the hydrodynamic radius which is defined by hypothetical hard sphere of the measured particles that comprises the metal nanoparticles and hydrated corona (Pryshchepa *et al*., 2020, Hemlata *et al*., 2020).

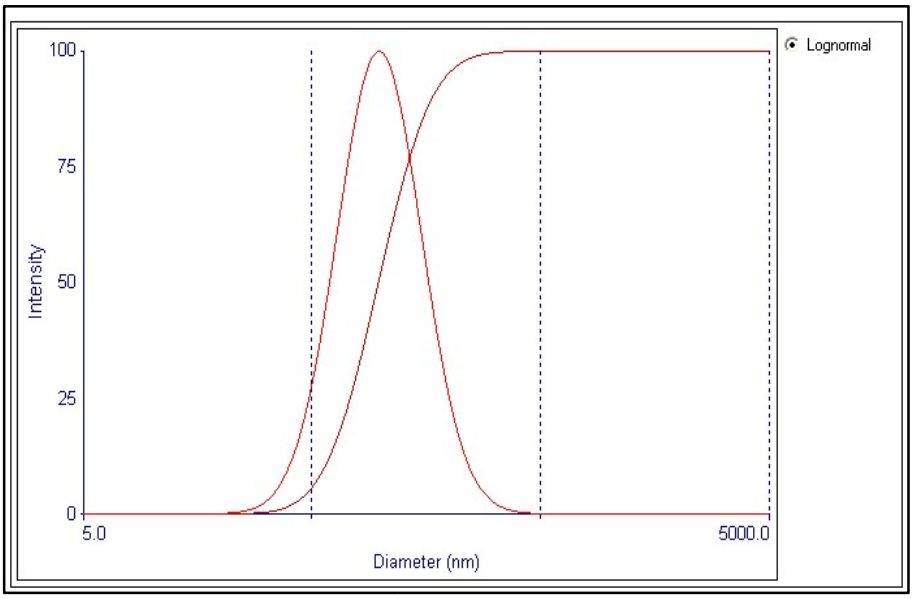

(A)

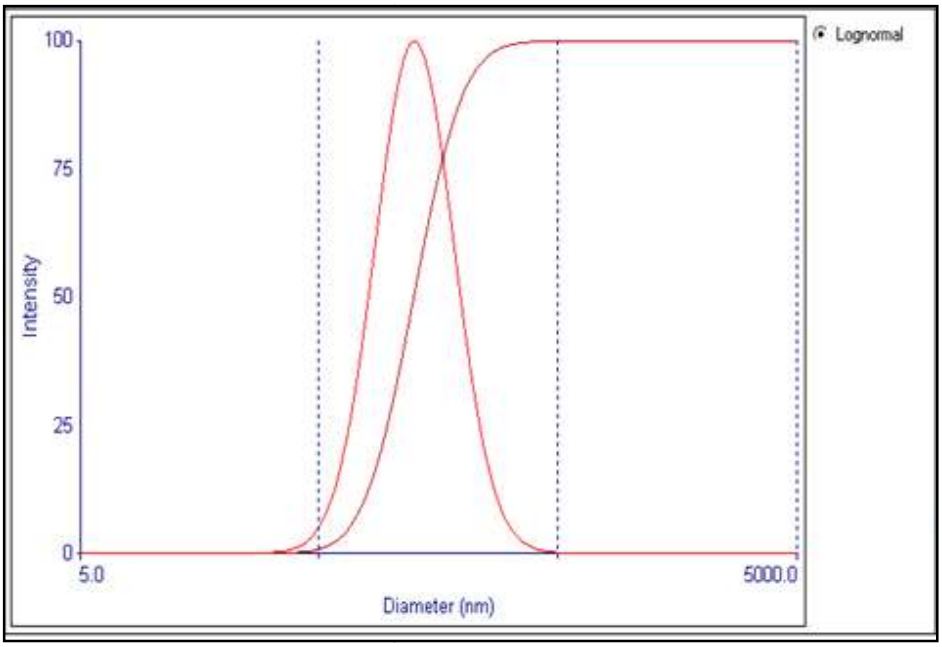

(B)

Figure 18: DLS size distribution diagram of (A) biosynthesized AgNPs and (B) AgNPs-Cip

3.5.4. Scanning electron microscopy (SEM)

As shown from the SEM images (Figure 19), spherical shaped AgNPs with large irregular clusters were synthesized. This may be due to the aggregation of particles through long storage and transportation. Since, the DLS result demonstrated that well distributed nanoparticles (PDI of 0.197 ± 0.009) were synthesized. The particles exhibited rough surface which is important to bacterial cell adhesion thereby causes a physical damage of bacterial cell wall, especially for gram negative bacteria which contain thin cell wall to be easily penetrated. This physical damage facilitate the bactericidal effect of the nanoparticles (Wu *et al.*, 2018).

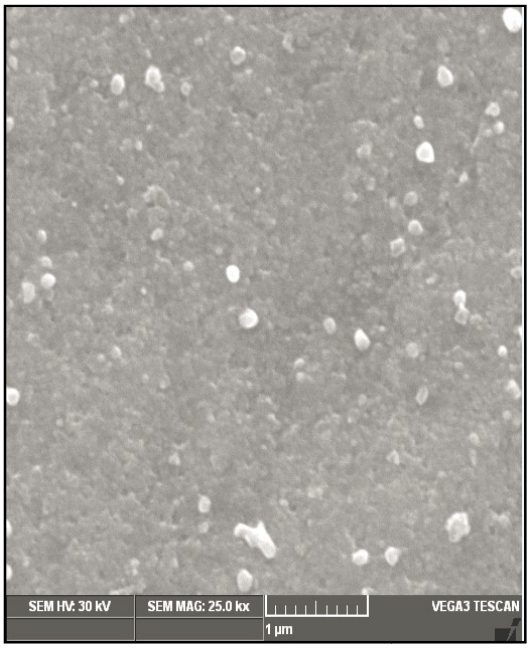

Average size =53 nm ± 0.02

(A)

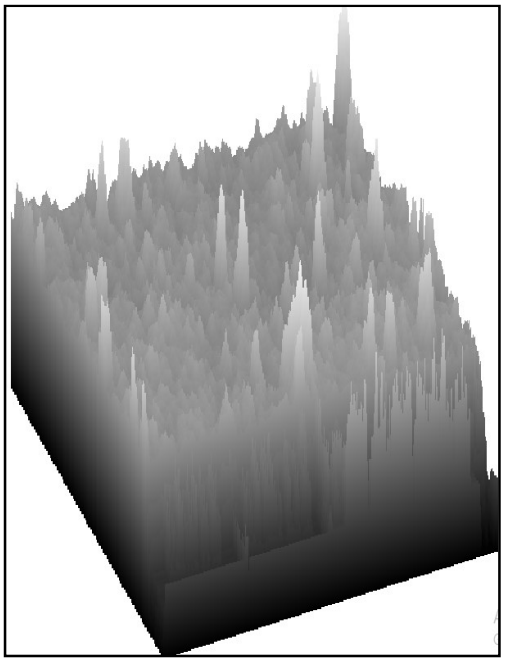

(B)

Figure 19: SEM micrographs of AgNPs (A) and its surface roughness (B)

3.5.5. X-ray diffraction (XRD)

The x-ray crystallography of synthesized AgNPs and the peak match comparison with the reference document (JCPDS 00-004-0783) is displayed in the Figure 20A and B, respectively. As revealed from the graph, four well resolved intense Bragg's reflections were appeared at 38.218 ^{o}, 43.855 ^{o}, 64.538 ^{o} and 77.374 ^{o} which were well matched with the reference (JCPDS 00-004-0783 with score of 85). These diffraction peaks indexed to the corresponding 111, 200, 220 and 311 lattice planes of face-centered-cubic (FCC) structure of AgNPs (Nogueira *et al*., 2014, Logaranjan *et al*., 2016, Huq, 2020). Some other smaller diffraction peaks displayed in the diffractogram were most probably attributed to the crystalline and amorphous phase of bio-organic molecules on the surface of AgNPs. Similar results were observed in previous XRD characterization of biosynthesized AgNPs by other researchers (Behravan *et al.*, 2019, Ulaeto *et al*., 2019, Awwad *et al.*, 2013).

As summarized in Table 2, the calculated average crystallite size of synthesized AgNPs was approximately 14 nm which is smaller than the size recorded by SEM. This might be due to the existence of twinned or poly-crystallites in a single nanoparticles core (Pryshchepa *et al*., 2020, Langford and Wilson, 1978).

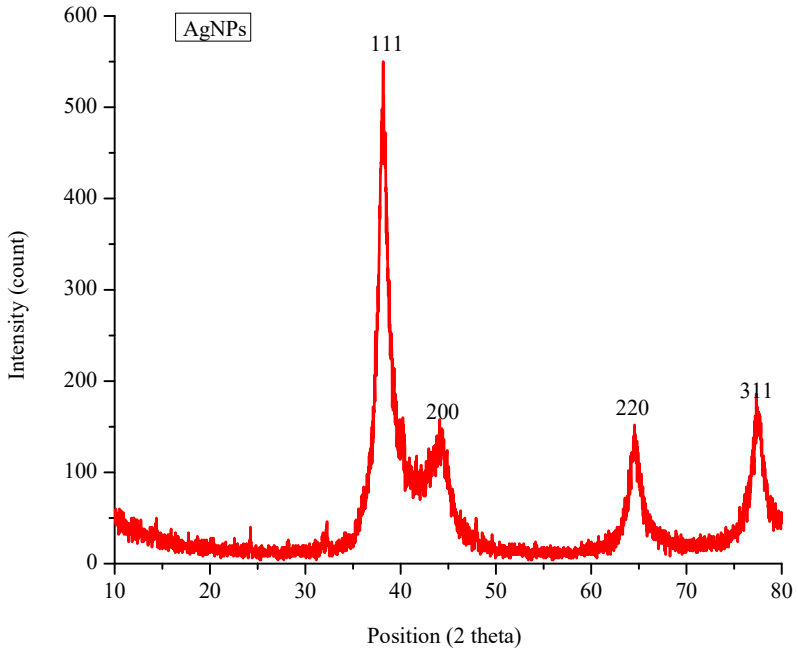

(A)

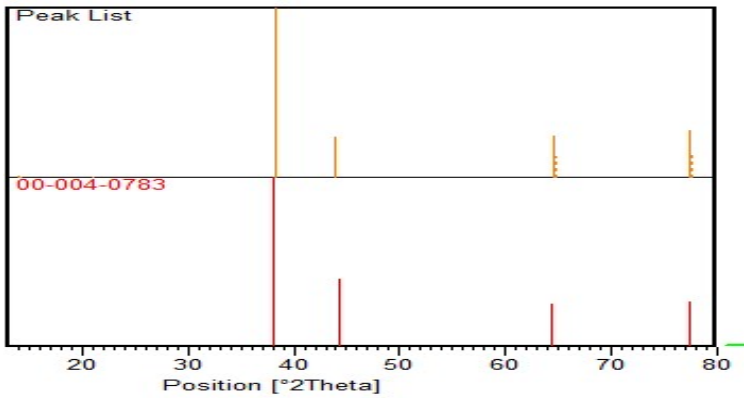

(B)

Figure 20: X-RD diffraction of AgNPs (A) major diffraction peaks by synthesized AgNPs and (B) diffraction peaks match with reference

Table 2: Summary of major crystallography peaks of biosynthesized AgNPs

Major peak list (arbitrary)	Position at 2 theta	FWHM	Crystallite size (nm)
1	38.218	1.698	10.50
2	43.9692	2.138	06.90
3	64.7175	1.502	15.60
4	77.6024	1.364	22.00
Average calculated crystallite size			13.75

3.5.6. Differential scanning calorimeter-thermogravimetric (DSC-TGA)

As the DSC-TGA thermograph (Figure 21) revealed, smaller percentage weight loss was occurred at temperature below 100 ^{o} C due to evaporation of adsorbed and entrapped water molecules (Abdul Kareem and Anu Kaliani, 2011). The graph of derivative weight (% / ^{o} C) also clearly indicated multistep decomposition phenomena at different temperatures. The weight losses between 100 and 350 ^{o} C attributed to the decomposition of flavonoids, phenols and carbohydrate which originate from the plant extract of *Aloe camperi* used in stabilization of AgNPs. Further steady weight loss was recorded above 350 ^{o} C. This might be due to thermal degradation of resistant aromatic compounds present on the surface of AgNPs (Moldovan *et al.*, 2018, David and Moldovan, 2020, Ulaeto *et al*., 2019). After complete decomposition, 88.71 % of the total mass was remained. The DSC thermograph also indicated that endothermic process. The endothermic peaks around 55 ^{o} C attributed to the elimination of moisture while the rest peaks might be due to the decomposition of organic molecules (David and Moldovan, 2020).

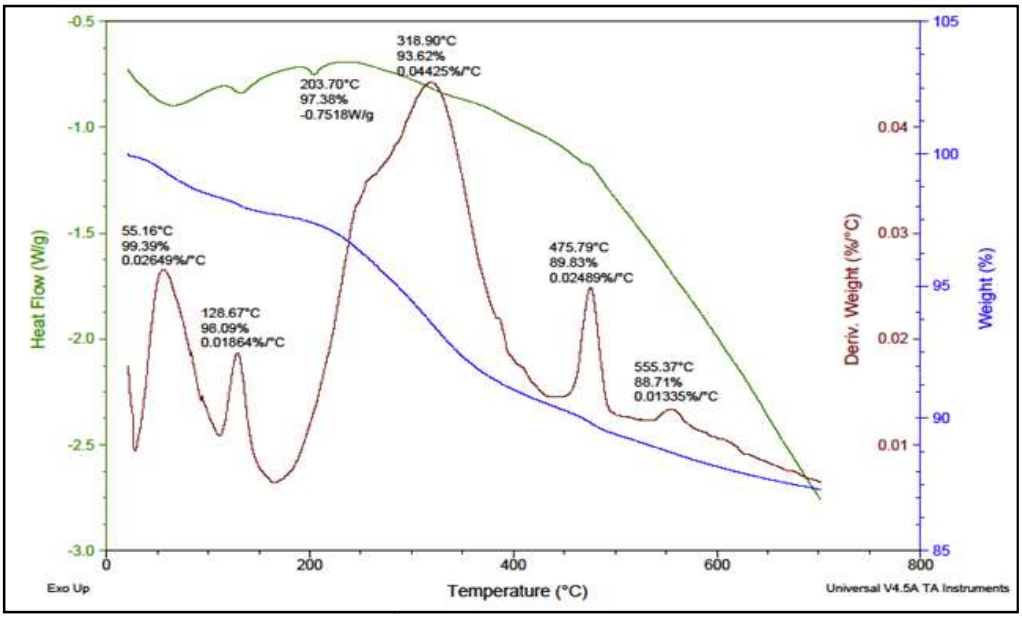

Figure 21: Simultaneous DSC-TGA graph of biosynthesized AgNPs

3.6. *In vitro* drug release study

Calibration curves of standard ciprofloxacin hydrochloride at four different pH (1.2, 6.0, 6.8 and 7.4) were constructed with linear equations and correlation coefficients of Y= 0.07099X + 0.00267; R^2 = 0.9995, Y = 0.07685X – 0.00101; R^2 =0.9999, Y = 0.06769X + 0.01643; R^2 = 0.9995 and Y= 0.06496X + 0.01663; R^2 = 0.9997, respectively (Appendix-2). Where Y, X and R^2 denoted absorbance, concentration and correlation coefficient as their order.

The graph which illustrated cumulative percentage release of ciprofloxacin hydrochloride from the loaded particles as a function of time, at four different pH media was plotted (Figure 22). As clearly observed from this graph, the release profile exhibited a biphasic pattern at all pH conditions. An initial burst release was observed for the first 4 hours then followed by slow release rate throughout the course of study. The rapid release phase might be in part due to the release of ciprofloxacin which was loosely adsorbed on the surface of AgNPs. Furthermore, due to the large surface area to volume ratio of the particles, the burst release of drug molecules might be triggered. This finding is in concordance with other reports on drug release profile from the surface of inorganic nanoparticles (Sreedharan and Singh, 2019, Shaker and Shaaban, 2017, England *et al.*, 2015). Moreover, the release rate was pH dependent. As shown from the graph, the fastest release was exhibited in acidic medium (pH-1.2). More than 76 % ± 0.8 and 91 % ± 0.3 of the total loaded drug content was released within 4 hours and 17 hours, respectively. In contrast, the slowest release was recorded at

highest pH medium (pH-7.4). At this condition, only 42 % ± 0.22 and 58 % ± 0.9 of the loaded content was released within 4 hours and 17 hours, respectively. This might be due to the inherent pH dependent solubility of ciprofloxacin which shows high solubility at pH values below 5 and above 10, and minimum solubility near the isoelectric point, which is close to neutral (Olivera *et al*., 2011). This implies at acidic medium (pH-1.2), the amine group at piperazine ring get protonated and possesses cationic property which may result in electrostatic repulsion with the cationic capping biomolecules. Even at slightly acidic medium (pH-6) which represents *E.coli* infected human bladder environment (Martín-Gutiérrez *et al.*, 2016), 67 % ± 0.9 and 83 % ± 1.3 of the loaded ciprofloxacin was released within 4 hours and 17 hours, respectively.

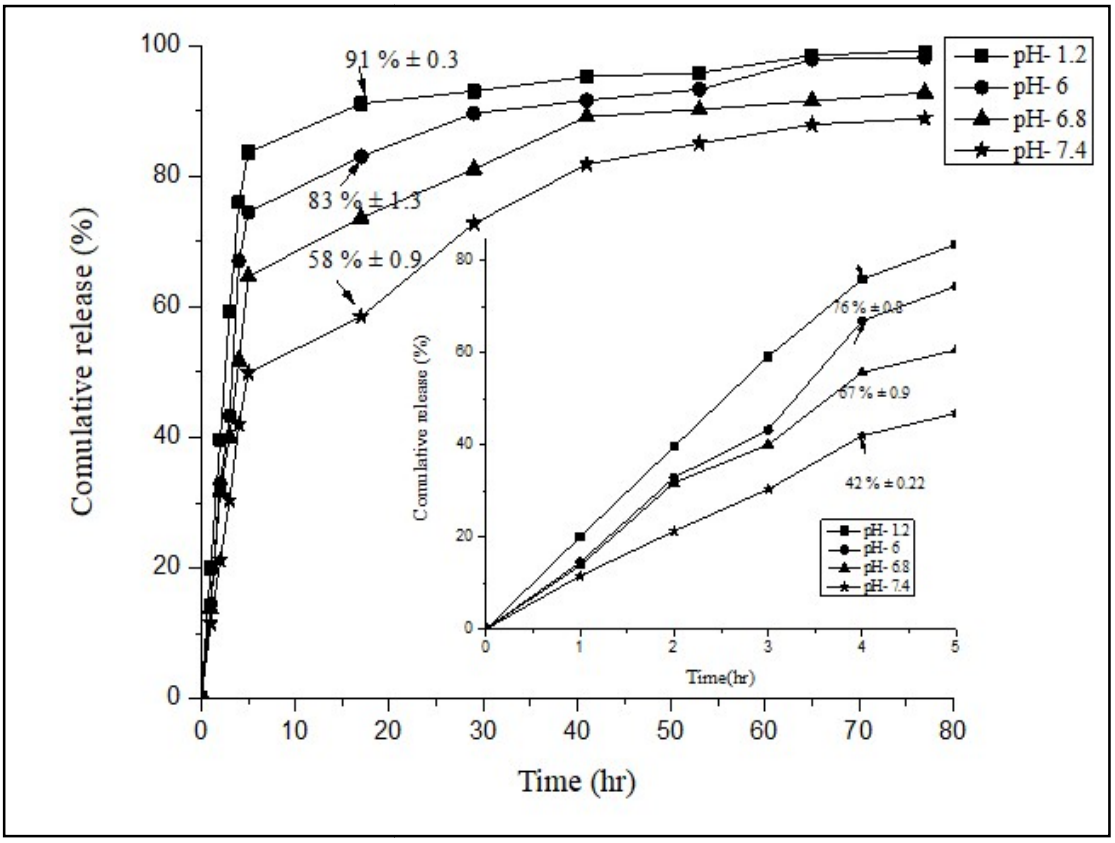

Figure 22: Graphs demonstrate the in vitro release of ciprofloxacin hydrochloride form biosynthesized AgNPs conjugate at different pH media. Where, the inset graphs illustrate only the first five hours releasing patterns.

3.7. *In vitro* antimicrobial susceptibility test

The results of disc diffusion tests demonstrated that the combination of ciprofloxacin with AgNPs augmented its efficacy. The effect of ciprofloxacin against resistant *E.coli* was enhanced through loading on the surface of AgNPs by the area fold increase of 0.99. Hence, the susceptibility of *E.coli* against ciprofloxacin was transformed from resistant to intermediate according to the classification of *in vitro* antimicrobial susceptibility test for ciprofloxacin (CLSI, 2020). This result is in agreement with a study report by Naqvi and collogues who evaluated the combined effects of different antibiotics, including ciprofloxacin with biosynthesized AgNPs against various multi-drug resistant bacteria. The result of disc diffusion test demonstrated an overall augmented effect with the average fold-area increase of 2.8. (Naqvi *et al.*, 2013). The possible explanation for this pronounced effect may be related to the different multimodal antibacterial action of AgNPs. Since, the variation in the mode of action of antibiotics and the nanoparticles enhance the susceptibility of the microbe. Besides

due to its hydrophobic nature, AgNPs act as a carrier to facilitate the transportation of ciprofloxacin hydrochloride to the bacterial cell membrane (Li *et al*., 2005). Despite an increase in ciprofloxacin efficacy through loading on AgNPs, the magnitude was not enough to turn the resistant pathogen into a complete susceptible one. This might be due to the smaller dose of AgNPs utilized in the current study, as only the standard dose of the drug for *in vitro* AST was considered. This means, the amount of loaded particles which incorporated 5 mg of ciprofloxacin was used in the disc diffusion tests. The average diameter of inhibition zones and the fold-area increase through loading were summarized in Table 3 below. As clearly shown from the table, the combination of ciprofloxacin with AgNPs improved its activity against resistant *E.coli*.

Table 3: Antimicrobial susceptibility test for AgNPs, ciprofloxacin and AgNPs-Cip

Material	Amount of loaded material per disc (mg)	Zone of inhibition (mm)	*In vitro* AST breaking point (CLSI, 2020)	Fold area increase
Control (0.85 % NS)		*6 ± 0.0	NA	
AgNPs	4.1	9 ± 0.6		0.99
Ciprofloxacin	5	17 ± 0.15	R	
AgNPs-Cip	9.1	24 ± 0.25	I	

Note: Breaking points: S: ≥26, I: 22-25, R: ≤ 21 mm^2 (CLSI, 2020), * 6 mm: diameter of disc, NA: not applicable

4. CONCLUSIONS

In this study, crystalline AgNPs with an average hydrodynamic diameter of 98.9 nm were successfully synthesized using the aqueous extract of *Aloe camperi*. Ciprofloxacin was also loaded effectively on the surface of synthesized nanoparticles without any surface modification. After loading on AgNPs, the susceptibility of *E.coli* against ciprofloxacin was transformed from resistant to intermediate according to the classification of in vitro antimicrobial susceptibility test breaking points for ciprofloxacin.

Therefore, the findings of this study demonstrate that biosynthesized AgNPs using *Aloe camperi* aqueous extract can be a potential nano carrier for ciprofloxacin delivery to improve its efficacy against resistant *E.coli*.

5. SUGGESTIONS FOR FURTHER WORK

The findings of the current study suggest in proceeding for further investigations in the following directions:

- Surface chemistry and stability studies
- *In vivo* efficacy and toxicity studies

6. REFERENCES

Abbas, M., Naeem, N., Iftikhar, H. & Latif, U. 2018. *Synthesis, characterization and antimicrobial properties of silver nanocomposites*, IntechOpen Limited; London, UK: 2018. Synthesis, characterization and antimicrobial properties of silver nanoparticles; pp. 71-91.

Abdul Kareem, T. & Anu Kaliani, A. 2011. Synthesis and thermal study of octahedral silver nano-plates in polyvinyl alcohol (PVA). *Arabian Journal of Chemistry*, 4, 325-331.

Abejew, A. A., Denboba, A. A. & Mekonnen, A. G. 2014. Prevalence and antibiotic resistance pattern of urinary tract bacterial infections in Dessie area, North-East Ethiopia. *BMC research notes,* 7**,** 1-7.

Adil, M., Khan, T., Aasim, M., Khan, A. A. & Ashraf, M. 2019. Evaluation of the antibacterial potential of silver nanoparticles synthesized through the interaction of antibiotic and aqueous callus extract of Fagonia indica. *AMB Express,* 9**,** 1-12.

Adom, D., Sekyere, P. A. & Krishnappa, M. K. 2020. The chemical constituents, anti-inflammatory, anti-oxidant, and ethnomedicinal properties of aloe barbadensis. *Ethnomedicinal Plant Use and Practice in Traditional Medicine.* IGI Global.

Agnihotri, S., Mukherji, S. & Mukherji, S. 2014. Size-controlled silver nanoparticles synthesized over the range 5–100 nm using the same protocol and their antibacterial efficacy. *Rsc Advances,* 4**,** 3974-3983.

Ahamed, M., Khan, M. M., Siddiqui, M., Alsalhi, M. S. & Alrokayan, S. A. 2011. Green synthesis, characterization and evaluation of biocompatibility of silver nanoparticles. *Physica E: Low-dimensional Systems and Nanostructures,* 43**,** 1266-1271.

Ahmad, A., Wei, Y., Syed, F., Tahir, K., Taj, R., Khan, A. U., Hameed, M. U. & Yuan, Q. 2016. Amphotericin B-conjugated biogenic silver nanoparticles as an innovative strategy for fungal infections. *Microbial pathogenesis,* 99**,** 271-281.

Ajitha, B., Reddy, Y. a. K. & Reddy, P. S. 2014. Biogenic nano-scale silver particles by Tephrosia purpurea leaf extract and their inborn antimicrobial activity. *Spectrochimica Acta Part A: Molecular and Biomolecular Spectroscopy,* 121**,** 164-172.

Akter, M., Sikder, M. T., Rahman, M. M., Ullah, A. A., Hossain, K. F. B., Banik, S., Hosokawa, T., Saito, T. & Kurasaki, M. 2018. A systematic review on silver nanoparticles-induced cytotoxicity: Physicochemical properties and perspectives. *Journal of advanced research,* 9**,** 1-16.

Alkawareek, M. Y., Bahlool, A., Abulateefeh, S. R. & Alkilany, A. M. 2019. Synergistic antibacterial activity of silver nanoparticles and hydrogen peroxide. *PloS one,* 14.

Allahverdiyev, A. M., Kon, K. V., Abamor, E. S., Bagirova, M. & Rafailovich, M. 2011. Coping with antibiotic resistance: combining nanoparticles with antibiotics and other antimicrobial agents. *Expert review of anti-infective therapy,* 9**,** 1035-1052.

Awwad, A. M., Salem, N. M. & Abdeen, A. O. 2013. Green synthesis of silver nanoparticles using carob leaf extract and its antibacterial activity. *International journal of Industrial chemistry,* 4**,** 1-6.

Baghizadeh, A., Ranjbar, S., Gupta, V. K., Asif, M., Pourseyedi, S., Karimi, M. J. & Mohammadinejad, R. 2015. Green synthesis of silver nanoparticles using seed extract of Calendula officinalis in liquid phase. *Journal of molecular liquids,* 207**,** 159-163.

Banu, K. S. & Cathrine, L. 2015. General techniques involved in phytochemical analysis. *International Journal of Advanced Research in Chemical Science,* 2**,** 25-32.

Behravan, M., Panahi, A. H., Naghizadeh, A., Ziaee, M., Mahdavi, R. & Mirzapour, A. 2019. Facile green synthesis of silver nanoparticles using Berberis vulgaris leaf and root aqueous extract and its antibacterial activity. *International journal of biological macromolecules,* 124**,** 148-154.

Benakashani, F., Allafchian, A. & Jalali, S. 2016. Biosynthesis of silver nanoparticles using Capparis spinosa L. leaf extract and their antibacterial activity. *Karbala International Journal of Modern Science,* 2**,** 251-258.

Beyene, G. & Tsegaye, W. 2011. Bacterial uropathogens in urinary tract infection and antibiotic susceptibility pattern in jimma university specialized hospital, southwest ethiopia. *Ethiopian journal of health sciences,* 21**,** 141-146.

Bhaumik, J., Thakur, N. S., Aili, P. K., Ghanghoriya, A., Mittal, A. K. & Banerjee, U. C. 2015. Bioinspired nanotheranostic agents: synthesis, surface functionalization, and antioxidant potential. *ACS Biomaterials Science & Engineering,* 1**,** 382-392.

Birla, S., Tiwari, V., Gade, A., Ingle, A., Yadav, A. & Rai, M. 2009. Fabrication of silver nanoparticles by Phoma glomerata and its combined effect against Escherichia coli, Pseudomonas aeruginosa and Staphylococcus aureus. *Letters in Applied Microbiology,* 48**,** 173-179.

Bisacchi, G. S. 2015. Origins of the quinolone class of antibacterials: an expanded "discovery story" miniperspective. *Journal of medicinal chemistry,* 58**,** 4874-4882.

Bitew, A., Molalign, T. & Chanie, M. 2017. Species distribution and antibiotic susceptibility profile of bacterial uropathogens among patients complaining urinary tract infections. *BMC infectious diseases,* 17**,** 1-8.

Blondeau, J. M. 2004. Fluoroquinolones: mechanism of action, classification, and development of resistance. *Survey of ophthalmology,* 49**,** S73-S78.

Bonde, S. 2011. A biogenic approach for green synthesis of silver nanoparticles using extract of Foeniculum vulgare and its activity against Staphylococcus aureus and Escherichia coli. *Nusantara Bioscience,* 3, 59-63.

Brauner, A., Fridman, O., Gefen, O. & Balaban, N. Q. 2016. Distinguishing between resistance, tolerance and persistence to antibiotic treatment. *Nature Reviews Microbiology,* 14**,** 320-330.

Burdușel, A.-C., Gherasim, O., Grumezescu, A. M., Mogoantă, L., Ficai, A. & Andronescu, E. 2018. Biomedical applications of silver nanoparticles: an up-to-date overview. *Nanomaterials,* 8**,** 681.

Cdc 2019. Antibiotic Resistance Threats in the United States 2019, Atlanta, GA: US Department of Health and Human Services, CDC; 2019.

Chouhan, N. 2018. Silver nanoparticles: Synthesis, characterization and applications. IntechOpen, PP 22-46.

Clsi 2020. Performance Standards for Antimicrobial Disk Susceptibility Tests; Approved Standard 40th ed. Clinical and Laboratory Standards Institute Wayne. PA.

Collignon, P. C., Conly, J. M., Andremont, A., Mcewen, S. A., Aidara-Kane, A., World Health Organization Advisory Group, B. M. O. I. S. O. a. R., Agerso, Y., Andremont, A., Collignon, P. & Conly, J. 2016. World Health Organization ranking of antimicrobials according to their importance in human medicine: a critical step for developing risk management strategies to control antimicrobial resistance from food animal production. *Clinical Infectious Diseases,* 63**,** 1087-1093.

Córdoba, G., Holm, A., Hansen, F., Hammerum, A. M. & Bjerrum, L. 2017. Prevalence of antimicrobial resistant Escherichia coli from patients with suspected urinary tract infection in primary care, Denmark. *BMC infectious diseases,* 17**,** 1-6.

Croxen, M. A., Law, R. J., Scholz, R., Keeney, K. M., Wlodarska, M. & Finlay, B. B. 2013. Recent advances in understanding enteric pathogenic Escherichia coli. *Clinical microbiology reviews,* 26**,** 822-880.

Cunha, F. A., Maia, K. R., Mallman, E. J. J., Cunha, M. D. C. D. S., Maciel, A. a. M., Souza, I. P. D., Menezes, E. A. & Fechine, P. B. A. 2016. Silver nanoparticles-disk diffusion

test against Escherichia coli isolates. *Revista do Instituto de Medicina Tropical de São Paulo,* 58.

Dada, A. O., Adekola, F. A., Adeyemi, O. S., Bello, O. M., Oluwaseun, A. C., Awakan, O. J. & Grace, F.-a. A. 2018. Exploring the effect of operational factors and characterization imperative to the synthesis of silver nanoparticles. *Silver Nanoparticles-Fabrication, Characterization and Applications.* IntechOpen.

David, L. & Moldovan, B. 2020. Green synthesis of biogenic silver nanoparticles for efficient catalytic removal of harmful organic dyes. *Nanomaterials,* 10**,** 202.

Deck, D. H. & Winston, L. G. 2012. Sulfonamides, trimethoprim, & quinolones. *Basic and clinical pharmacology*.

Demissew, S., Nordal, I. & Stabbetorp, O. E. 2001. Endemism and patterns of distribution of the genus Aloe (Aloaceae) in the flora of Ethiopia and Eritrea. *Biologiske Skrifter,* 54**,** 233-246.

Demoz, M. S., Gachoki, K. P., Mungai, K. J. & Negusse, B. G. 2015. Ethnobotanical survey and preliminary phytochemical studies of plants traditionally used for diabetes in eritrea. *European Journal of Medicinal Plants***,** 1-11.

Doma, A. O., Popescu, R., Mituleţu, M., Muntean, D., Dégi, J., Boldea, M. V., Radulov, I., Dumitrescu, E., Muselin, F. & Puvača, N. 2020. Comparative Evaluation of qnrA, qnrB, and qnrS Genes in Enterobacteriaceae Ciprofloxacin-Resistant Cases, in Swine Units and a Hospital from Western Romania. *Antibiotics,* 9**,** 698.

Durán, N., Marcato, P. D., Conti, R. D., Alves, O. L., Costa, F. & Brocchi, M. 2010. Potential use of silver nanoparticles on pathogenic bacteria, their toxicity and possible mechanisms of action. *Journal of the Brazilian Chemical Society,* 21**,** 949-959.

Ecdc/Efsa/Ema 2017. ECDC/EFSA/EMA second joint report on the integrated analysis of the consumption of antimicrobial agents and occurrence of antimicrobial resistance in bacteria from humans and food-producing animals: Joint Interagency Antimicrobial Consumption and Resistance Analysis (JIACRA) Report. *EFSA Journal,* 15**,** e04872.

Efmhaca 2013. Medicine and Healthcare Administration and Control Authority. *Continuing Professional Development [CPD] guideline for health professionals in Ethiopia. Addis Ababa, Ethiopia: Federal Democratic Republic of Ethiopia Ministry of Health*.

Elkhatim, F. S., Issa, T. O., Suliman, S. I., Mohamed, Y. S., Makhawi, A. M. & Khider, T. O. 2019. Phytochemical Screening and Antimicrobial Activity of Different Extractions of Sudanese Stylochiton borumensis Roots (Araceae). *World Applied Sciences Journal,* 37**,** 700-709.

Emasushan, M. & Britto, J. 2018. Preliminary phytochemical profiling and antifungal activity of the seeds and pericarp of Putranjiva roxburghii Wall. *The Pharma Innovation Journal,* 7**,** 107-110.

England, C. G., Miller, M. C., Kuttan, A., Trent, J. O. & Frieboes, H. B. 2015. Release kinetics of paclitaxel and cisplatin from two and three layered gold nanoparticles. *European Journal of Pharmaceutics and Biopharmaceutics,* 92**,** 120-129.

Ephi 2020. Ethiopia Antimicrobial Resistance Surveillance Annual Report (2nd Year) September 2018 – October 2019. Addis Ababa.

Fda 2016. Highlights of prescribing information These highlights do not include all the information needed to use CIPROFLOXACIN Tablets, USP safely and effectively. See full prescribing information for CIPROFLOXACIN Tablets, USP. CIPROFLOXACIN Tablets, USP (ciprofloxacin hydrochloride) tablet, for oral use.

Flores-Mireles, A. L., Walker, J. N., Caparon, M. & Hultgren, S. J. 2015. Urinary tract infections: epidemiology, mechanisms of infection and treatment options. *Nature reviews microbiology,* 13**,** 269-284.

From, C. O. S. N. 2016. Withania Somnifera (L.) Dunal. *Asian J Pharm Clin Res,* 9**,** 34-39.

García, M. A. 2011. Surface plasmons in metallic nanoparticles: fundamentals and applications. *Journal of Physics D: Applied Physics,* 44**,** 283001.

Ghiuță, I., Cristea, D., Croitoru, C., Kost, J., Wenkert, R., Vyrides, I., Anayiotos, A. & Munteanu, D. 2018. Characterization and antimicrobial activity of silver nanoparticles, biosynthesized using Bacillus species. *Applied Surface Science,* 438**,** 66-73.

Gomes, H. I., Martins, C. S. & Prior, J. A. 2021. Silver Nanoparticles as Carriers of Anticancer Drugs for Efficient Target Treatment of Cancer Cells. *Nanomaterials,* 11**,** 964.

Gu, C. & Karthikeyan, K. 2005. Sorption of the antimicrobial ciprofloxacin to aluminum and iron hydrous oxides. *Environmental science & technology,* 39**,** 9166-9173.

Gul, R., Jan, S. U., Faridullah, S., Sherani, S. & Jahan, N. 2017. Preliminary phytochemical screening, quantitative analysis of alkaloids, and antioxidant activity of crude plant extracts from Ephedra intermedia indigenous to Balochistan. *The Scientific World Journal,* 2017.

Hadrup, N. & Lam, H. R. 2014. Oral toxicity of silver ions, silver nanoparticles and colloidal silver–a review. *Regulatory Toxicology and Pharmacology,* 68**,** 1-7.

Harshiny, M., Matheswaran, M., Arthanareeswaran, G., Kumaran, S. & Rajasree, S. 2015. Enhancement of antibacterial properties of silver nanoparticles–ceftriaxone conjugate through Mukia maderaspatana leaf extract mediated synthesis. *Ecotoxicology and environmental safety,* 121**,** 135-141.

Hay, S. I., Rao, P. C., Dolecek, C., Day, N. P., Stergachis, A., Lopez, A. D. & Murray, C. J. 2018. Measuring and mapping the global burden of antimicrobial resistance. *BMC medicine,* 16**,** 78.

Hemlata, Meena, P. R., Singh, A. P. & Tejavath, K. K. 2020. Biosynthesis of silver nanoparticles using cucumis prophetarum aqueous leaf extract and their antibacterial and antiproliferative activity against cancer cell lines. *ACS omega,* 5**,** 5520-5528.

Hooper, D. C. & Jacoby, G. A. 2016. Topoisomerase inhibitors: fluoroquinolone mechanisms of action and resistance. *Cold Spring Harbor perspectives in medicine,* 6**,** a025320.

Huang, J., Zhan, G., Zheng, B., Sun, D., Lu, F., Lin, Y., Chen, H., Zheng, Z., Zheng, Y. & Li, Q. 2011. Biogenic silver nanoparticles by Cacumen platycladi extract: synthesis, formation mechanism, and antibacterial activity. *Industrial & engineering chemistry research,* 50**,** 9095-9106.

Huq, M. 2020. Green synthesis of silver nanoparticles using Pseudoduganella eburnea MAHUQ-39 and their antimicrobial mechanisms investigation against drug resistant human pathogens. *International journal of molecular sciences,* 21**,** 1510.

Ibrahim, E. H., Kilany, M., Ghramh, H. A., Khan, K. A. & Ul Islam, S. 2019. Cellular proliferation/cytotoxicity and antimicrobial potentials of green synthesized silver nanoparticles (AgNPs) using Juniperus procera. *Saudi journal of biological sciences,* 26**,** 1689-1694.

Ibrahim, H. M. 2015. Green synthesis and characterization of silver nanoparticles using banana peel extract and their antimicrobial activity against representative microorganisms. *Journal of Radiation Research and Applied Sciences,* 8**,** 265-275.

Iravani, S., Korbekandi, H., Mirmohammadi, S. V. & Zolfaghari, B. 2014. Synthesis of silver nanoparticles: chemical, physical and biological methods. *Research in pharmaceutical sciences,* 9**,** 385.

Ivanova, N., Gugleva, V., Dobreva, M., Pehlivanov, I., Stefanov, S. & Andonova, V. 2018. Silver nanoparticles as multi-functional drug delivery systems. *Nanomedicines.* IntechOpen.

Jacoby, G. A., Strahilevitz, J. & Hooper, D. C. 2015. Plasmid-mediated quinolone resistance. *Plasmids: Biology and Impact in Biotechnology and Discovery***,** 475-503.

Jain, S. & Mehata, M. S. 2017. Medicinal plant leaf extract and pure flavonoid mediated green synthesis of silver nanoparticles and their enhanced antibacterial property. *Scientific reports,* 7**,** 1-13.

Jamkhande, P. G., Ghule, N. W., Bamer, A. H. & Kalaskar, M. G. 2019. Metal nanoparticles synthesis: An overview on methods of preparation, advantages and disadvantages, and applications. *Journal of Drug Delivery Science and Technology,* 53**,** 101174.

Jelinkova, P., Mazumdar, A., Sur, V. P., Kociova, S., Dolezelikova, K., Jimenez, A. M. J., Koudelkova, Z., Mishra, P. K., Smerkova, K. & Heger, Z. 2019. Nanoparticle-drug conjugates treating bacterial infections. *Journal of Controlled Release*.

Kabew, G., Abebe, T. & Miheret, A. 2013. A retrospective study on prevalence and antimicrobial susceptibility patterns of bacterial isolates from urinary tract infections in Tikur Anbessa Specialized Teaching Hospital Addis Ababa, Ethiopia, 2011. *Ethiopian Journal of Health Development,* 27**,** 111-117.

Kim, M., Osone, S., Kim, T., Higashi, H. & Seto, T. 2017. Synthesis of nanoparticles by laser ablation: A review. *KONA Powder and Particle Journal***,** 2017009.

Kim, T. Y., Cha, S.-H., Cho, S. & Park, Y. 2016. Tannic acid-mediated green synthesis of antibacterial silver nanoparticles. *Archives of pharmacal research,* 39**,** 465-473.

Kim, Y. S., Kim, J. S., Cho, H. S., Rha, D. S., Kim, J. M., Park, J. D., Choi, B. S., Lim, R., Chang, H. K. & Chung, Y. H. 2008. Twenty-eight-day oral toxicity, genotoxicity, and gender-related tissue distribution of silver nanoparticles in Sprague-Dawley rats. *Inhalation toxicology,* 20**,** 575-583.

Klein, E. Y., Van Boeckel, T. P., Martinez, E. M., Pant, S., Gandra, S., Levin, S. A., Goossens, H. & Laxminarayan, R. 2018. Global increase and geographic convergence in antibiotic consumption between 2000 and 2015. *Proceedings of the National Academy of Sciences,* 115**,** E3463-E3470.

Kobayashi, M., Shapiro, D. J., Hersh, A. L., Sanchez, G. V. & Hicks, L. A. Outpatient antibiotic prescribing practices for uncomplicated urinary tract infection in women in the United States, 2002–2011. Open forum infectious diseases, 2016. Oxford University Press, ofw159.

Kudinha, T. 2017. The pathogenesis of Escherichia coli urinary tract infection. *Escherichia coli—Recent Advances on Physiology, Pathogenesis and Biotechnological Applications. InTech***,** 45-61.

Langford, J. I. & Wilson, A. 1978. Scherrer after sixty years: a survey and some new results in the determination of crystallite size. *Journal of applied crystallography,* 11**,** 102-113.

Lavanya, M., Veenavardhini, S. V., Gim, G. H., Kathiravan, M. N. & Kim, S. W. 2013. Synthesis, characterization and evaluation of antimicrobial efficacy of silver nanoparticles using Paederia foetida L. leaf extract. *Int res j biol,* 2**,** 28-34.

Lea, M. C. 1889. ART. L.--On Allotropic Forms of Silver. *American Journal of Science (1880-1910),* 37**,** 476.

Lebel, M. 1988. Ciprofloxacin: chemistry, mechanism of action, resistance, antimicrobial spectrum, pharmacokinetics, clinical trials, and adverse reactions. *Pharmacotherapy: The Journal of Human Pharmacology and Drug Therapy,* 8**,** 3-30.

Lee, S. H. & Jun, B.-H. 2019. Silver Nanoparticles: Synthesis and application for nanomedicine. *International journal of molecular sciences,* 20**,** 865.

Li, P., Li, J., Wu, C., Wu, Q. & Li, J. 2005. Synergistic antibacterial effects of β-lactam antibiotic combined with silver nanoparticles. *Nanotechnology,* 16**,** 1912.

Li, W.-R., Sun, T.-L., Zhou, S.-L., Ma, Y.-K., Shi, Q.-S., Xie, X.-B. & Huang, X.-M. 2017. A comparative analysis of antibacterial activity, dynamics, and effects of silver ions and silver nanoparticles against four bacterial strains. *International Biodeterioration & Biodegradation,* 123**,** 304-310.

Li, W.-R., Xie, X.-B., Shi, Q.-S., Zeng, H.-Y., You-Sheng, O.-Y. & Chen, Y.-B. 2010. Antibacterial activity and mechanism of silver nanoparticles on Escherichia coli. *Applied microbiology and biotechnology,* 85**,** 1115-1122.

Li, Z., Hong, H., Liao, L., Ackley, C. J., Schulz, L. A., Macdonald, R. A., Mihelich, A. L. & Emard, S. M. 2011. A mechanistic study of ciprofloxacin removal by kaolinite. *Colloids and Surfaces B: Biointerfaces,* 88**,** 339-344.

Logaranjan, K., Raiza, A. J., Gopinath, S. C., Chen, Y. & Pandian, K. 2016. Shape-and size-controlled synthesis of silver nanoparticles using Aloe vera plant extract and their antimicrobial activity. *Nanoscale research letters,* 11**,** 1-9.

Lok, C.-N., Ho, C.-M., Chen, R., He, Q.-Y., Yu, W.-Y., Sun, H., Tam, P. K.-H., Chiu, J.-F. & Che, C.-M. 2006. Proteomic analysis of the mode of antibacterial action of silver nanoparticles. *Journal of proteome research,* 5**,** 916-924.

Lopez-Carrizales, M., Velasco, K. I., Castillo, C., Flores, A., Magaña, M., Martinez-Castanon, G. A. & Martinez-Gutierrez, F. 2018. In vitro synergism of silver

nanoparticles with antibiotics as an alternative treatment in multiresistant uropathogens. *Antibiotics,* 7**,** 50.

Malapermal, V., Botha, I., Krishna, S. B. N. & Mbatha, J. N. 2017. Enhancing antidiabetic and antimicrobial performance of Ocimum basilicum, and Ocimum sanctum (L.) using silver nanoparticles. *Saudi journal of biological sciences,* 24**,** 1294-1305.

Marciniak, L., Nowak, M., Trojanowska, A., Tylkowski, B. & Jastrzab, R. 2020. The effect of pH on the size of silver nanoparticles obtained in the reduction reaction with citric and malic acids. *Materials,* 13**,** 5444.

Martín-Gutiérrez, G., Rodríguez-Beltrán, J., Rodríguez-Martínez, J. M., Costas, C., Aznar, J., Pascual, Á. & Blázquez, J. 2016. Urinary tract physiological conditions promote ciprofloxacin resistance in low-level-quinolone-resistant Escherichia coli. *Antimicrobial agents and chemotherapy,* 60**,** 4252-4258.

Mcshan, D., Zhang, Y., Deng, H., Ray, P. C. & Yu, H. 2015. Synergistic antibacterial effect of silver nanoparticles combined with ineffective antibiotics on drug resistant Salmonella typhimurium DT104. *Journal of Environmental Science and Health, Part C,* 33**,** 369-384.

Medhin, L. B., Sibhatu, D. B., Seid, M., Ferej, F. M., Mohamedkassm, N., Berhane, Y., Kaushek, A., Humida, M. E. & Gasmalbari, E. 2019. Comparative antimicrobial activities of the gel, leaf and anthraquinone fractionates of four Aloe Species (Aloe camperi, Aloe elegans, Aloe eumassawana and Aloe scholleri). *Advances in Microbiology,* 9**,** 139-150.

Megeressa, M., Bisrat, D., Mazumder, A. & Asres, K. 2015. Structural elucidation of some antimicrobial constituents from the leaf latex of Aloe trigonantha LC Leach. *BMC Complementary and Alternative Medicine,* 15**,** 1-7.

Mohsen, E., El-Borady, O. M., Mohamed, M. B. & Fahim, I. S. 2020. Synthesis and characterization of ciprofloxacin loaded silver nanoparticles and investigation of their antibacterial effect. *Journal of Radiation Research and Applied Sciences,* 13**,** 416-425.

Moldovan, B., Sincari, V., Perde-Schrepler, M. & David, L. 2018. Biosynthesis of silver nanoparticles using Ligustrum ovalifolium fruits and their cytotoxic effects. *Nanomaterials,* 8**,** 627.

Muggeo, A., Cambau, E., Amara, M., Micaëlo, M., Pangon, B., Bajolet, O., Benmansour, H., De Champs, C. & Guillard, T. 2020. Phenotypic and genotypic quinolone resistance

in Escherichia coli underlining GyrA83/87 mutations as a target to detect ciprofloxacin resistance. *Journal of Antimicrobial Chemotherapy,* 75**,** 2466-2470.

Munger, M. A., Radwanski, P., Hadlock, G. C., Stoddard, G., Shaaban, A., Falconer, J., Grainger, D. W. & Deering-Rice, C. E. 2014. In vivo human time-exposure study of orally dosed commercial silver nanoparticles. *Nanomedicine: Nanotechnology, Biology and Medicine,* 10**,** 1-9.

Murei, A., Ayinde, W. B., Gitari, M. W. & Samie, A. 2020. Functionalization and antimicrobial evaluation of ampicillin, penicillin and vancomycin with Pyrenacantha grandiflora Baill and silver nanoparticles. *Scientific Reports,* 10**,** 1-14.

Naqvi, S. Z. H., Kiran, U., Ali, M. I., Jamal, A., Hameed, A., Ahmed, S. & Ali, N. 2013. Combined efficacy of biologically synthesized silver nanoparticles and different antibiotics against multidrug-resistant bacteria. *International journal of nanomedicine,* 8**,** 3187.

Nogueira, A. L., Machado, R. A., De Souza, A. Z., Martinello, F. V., Franco, C. S. V. & Dutra, G. B. 2014. Synthesis and characterization of silver nanoparticles produced with a bifunctional stabilizing agent. *Industrial & Engineering Chemistry Research,* 53**,** 3426-3434.

Nowack, B., Krug, H. F. & Height, M. 2011. 120 years of nanosilver history: implications for policy makers. ACS Publications.

Oda, B. K. & Erena, B. A. 2017. Aloesof Ethiopia: A Review on Uses and Importance of Aloes in Ethiopia. *Int J Plant Biol Res,* 5**,** 1059.

Olivera, M. E., Manzo, R. H., Junginger, H., Midha, K., Shah, V., Stavchansky, S., Dressman, J. & Barends, D. 2011. Biowaiver monographs for immediate release solid oral dosage forms: Ciprofloxacin hydrochloride. *Journal of pharmaceutical sciences,* 100**,** 22-33.

Otunola, G. A., Afolayan, A. J., Ajayi, E. O. & Odeyemi, S. W. 2017. Characterization, antibacterial and antioxidant properties of silver nanoparticles synthesized from aqueous extracts of Allium sativum, Zingiber officinale, and Capsicum frutescens. *Pharmacognosy magazine,* 13**,** S201.

Ovais, M., Khalil, A. T., Islam, N. U., Ahmad, I., Ayaz, M., Saravanan, M., Shinwari, Z. K. & Mukherjee, S. 2018. Role of plant phytochemicals and microbial enzymes in biosynthesis of metallic nanoparticles. *Applied microbiology and biotechnology,* 102**,** 6799-6814.

Parveen, K., Banse, V. & Ledwani, L. Green synthesis of nanoparticles: their advantages and disadvantages. AIP conference proceedings, 2016. AIP Publishing LLC, 020048.

Pataki, B. Á., Matamoros, S., Van Der Putten, B. C., Remondini, D., Giampieri, E., Aytan-Aktug, D., Hendriksen, R. S., Lund, O., Csabai, I. & Schultsz, C. 2020. Understanding and predicting ciprofloxacin minimum inhibitory concentration in Escherichia coli with machine learning. *Scientific reports,* 10**,** 1-9.

Patra, J. K. & Baek, K.-H. 2014. Green nanobiotechnology: factors affecting synthesis and characterization techniques. *Journal of Nanomaterials,* 2014.

Peiris, S., Mcmurtrie, J. & Zhu, H.-Y. 2016. Metal nanoparticle photocatalysts: emerging processes for green organic synthesis. *Catalysis Science & Technology,* 6**,** 320-338.

Perveen, S., Safdar, N. & Yasmin, A. 2018. Antibacterial evaluation of silver nanoparticles synthesized from lychee peel: individual versus antibiotic conjugated effects. *World Journal of Microbiology and Biotechnology,* 34**,** 1-12.

Prabhu, S. & Poulose, E. K. 2012. Silver nanoparticles: mechanism of antimicrobial action, synthesis, medical applications, and toxicity effects. *International nano letters,* 2**,** 32.

Prasad, S. R., Elango, K., Damayanthi, D. & Saranya, J. 2013. Formulation and evaluation of azathioprine loaded silver nanopartilces for the treatment of rheumatoid arthritis. *AJBPS,* 3**,** 28-32.

Praski Alzrigat, L., Huseby, D. L., Brandis, G. & Hughes, D. 2021. Resistance/fitness trade-off is a barrier to the evolution of MarR inactivation mutants in Escherichia coli. *Journal of Antimicrobial Chemotherapy,* 76**,** 77-83.

Pryshchepa, O., Pomastowski, P. & Buszewski, B. 2020. Silver nanoparticles: Synthesis, investigation techniques, and properties. *Advances in Colloid and Interface Science***,** 102246.

Qureshi, A. T. 2013. Silver Nanoparticles As Drug Delivery Systems.

Radzig, M., Nadtochenko, V., Koksharova, O., Kiwi, J., Lipasova, V. & Khmel, I. 2013. Antibacterial effects of silver nanoparticles on gram-negative bacteria: influence on the growth and biofilms formation, mechanisms of action. *Colloids and Surfaces B: Biointerfaces,* 102**,** 300-306.

Rai, M., Deshmukh, S., Ingle, A. & Gade, A. 2012. Silver nanoparticles: the powerful nanoweapon against multidrug-resistant bacteria. *Journal of applied microbiology,* 112**,** 841-852.

Raj, S., Singh, H., Trivedi, R. & Soni, V. 2020. Biogenic synthesis of AgNPs employing Terminalia arjuna leaf extract and its efficacy towards catalytic degradation of organic dyes. *Scientific Reports,* 10**,** 1-10.

Roe, D., Karandikar, B., Bonn-Savage, N., Gibbins, B. & Roullet, J.-B. 2008. Antimicrobial surface functionalization of plastic catheters by silver nanoparticles. *Journal of antimicrobial chemotherapy,* 61**,** 869-876.

Roldán, M. V., Scaffardi, L. B., De Sanctis, O. & Pellegri, N. 2008. Optical properties and extinction spectroscopy to characterize the synthesis of amine capped silver nanoparticles. *Materials Chemistry and Physics,* 112**,** 984-990.

Roni, M., Murugan, K., Panneerselvam, C., Subramaniam, J. & Hwang, J.-S. 2013. Evaluation of leaf aqueous extract and synthesized silver nanoparticles using Nerium oleander against Anopheles stephensi (Diptera: Culicidae). *Parasitology Research,* 112**,** 981-990.

Rout, A., Jena, P. K., Sahoo, D. & Bindhani, B. K. 2014. Green synthesis of silver nanoparticles of different shapes and its antibacterial activity against Escherichia coli. *Int. J. Curr. Microbiol. App. Sci,* 3**,** 374-383.

Roy, A., Bulut, O., Some, S., Mandal, A. K. & Yilmaz, M. D. 2019. Green synthesis of silver nanoparticles: biomolecule-nanoparticle organizations targeting antimicrobial activity. *RSC advances,* 9**,** 2673-2702.

Sadat Shandiz, S. A., Shafiee Ardestani, M., Shahbazzadeh, D., Assadi, A., Ahangari Cohan, R., Asgary, V. & Salehi, S. 2017. Novel imatinib-loaded silver nanoparticles for enhanced apoptosis of human breast cancer MCF-7 cells. *Artificial cells, nanomedicine, and biotechnology,* 45**,** 1082-1091.

Sahoo, S., Chakraborti, C. K., Mishra, S. C., Nanda, U. & Naik, S. 2011. FTIR and XRD investigations of some fluoroquinolones.

Sanchooli, N., Saeidi, S., Barani, H. K. & Sanchooli, E. 2018. In vitro antibacterial effects of silver nanoparticles synthesized using Verbena officinalis leaf extract on Yersinia ruckeri, Vibrio cholera and Listeria monocytogenes. *Iranian journal of microbiology,* 10**,** 400.

Sangeetha, J., Sandhya, J. & Philip, J. 2014. Biosynthesis and Functionalization of Silver Nanoparticles Using Nigellasativa, Dioscorea alata and Ferula asafoetida. *Science of Advanced Materials,* 6**,** 1681-1690.

Segura, R., Vásquez, G., Colson, E., Gerbaux, P., Frischmon, C., Nesic, A., García, D. E. & Cabrera-Barjas, G. 2020. Phytostimulant properties of highly stable silver

nanoparticles obtained with saponin extract from Chenopodium quinoa. *Journal of the Science of Food and Agriculture,* 100**,** 4987-4994.

Seifu, W. D. & Gebissa, A. D. 2018. Prevalence and antibiotic susceptibility of Uropathogens from cases of urinary tract infections (UTI) in Shashemene referral hospital, Ethiopia. *BMC infectious diseases,* 18**,** 1-9.

Selvan, D. A., Mahendiran, D., Kumar, R. S. & Rahiman, A. K. 2018. Garlic, green tea and turmeric extracts-mediated green synthesis of silver nanoparticles: Phytochemical, antioxidant and in vitro cytotoxicity studies. *Journal of Photochemistry and Photobiology B: Biology,* 180**,** 243-252.

Shaker, M. A. & Shaaban, M. I. 2017. Formulation of carbapenems loaded gold nanoparticles to combat multi-antibiotic bacterial resistance: in vitro antibacterial study. *International journal of pharmaceutics,* 525**,** 71-84.

Shameli, K., Ahmad, M. B., Jazayeri, S. D., Shabanzadeh, P., Sangpour, P., Jahangirian, H. & Gharayebi, Y. 2012. Investigation of antibacterial properties silver nanoparticles prepared via green method. *Chemistry Central Journal,* 6**,** 73.

Singh, P., Kim, Y.-J., Zhang, D. & Yang, D.-C. 2016. Biological synthesis of nanoparticles from plants and microorganisms. *Trends in biotechnology,* 34**,** 588-599.

Song, J. Y. & Kim, B. S. 2009. Rapid biological synthesis of silver nanoparticles using plant leaf extracts. *Bioprocess and biosystems engineering,* 32**,** 79.

Soucy, J.-P. R., Schmidt, A. M., Quach, C. & Buckeridge, D. L. 2020. Fluoroquinolone Use and Seasonal Patterns of Ciprofloxacin Resistance in Community-Acquired Urinary Escherichia coli Infection in a Large Urban Center. *American journal of epidemiology,* 189**,** 215-223.

Spellberg, B. & Doi, Y. 2015. The Rise of Fluoroquinolone-Resistant E. coli in the Community: Scarier than We Thought.

Sreedharan, S. M. & Singh, R. 2019. Ciprofloxacin Functionalized Biogenic Gold Nanoflowers as Nanoantibiotics Against Pathogenic Bacterial Strains. *International Journal of Nanomedicine,* 14**,** 9905.

Stensberg, M. C., Wei, Q., Mclamore, E. S., Porterfield, D. M., Wei, A. & Sepúlveda, M. S. 2011. Toxicological studies on silver nanoparticles: challenges and opportunities in assessment, monitoring and imaging. *Nanomedicine,* 6**,** 879-898.

Sun, Q., Cai, X., Li, J., Zheng, M., Chen, Z. & Yu, C.-P. 2014. Green synthesis of silver nanoparticles using tea leaf extract and evaluation of their stability and antibacterial

activity. *Colloids and surfaces A: Physicochemical and Engineering aspects,* 444**,** 226-231.

Sung, J. H., Ji, J. H., Park, J. D., Yoon, J. U., Kim, D. S., Jeon, K. S., Song, M. Y., Jeong, J., Han, B. S. & Han, J. H. 2009. Subchronic inhalation toxicity of silver nanoparticles. *Toxicological sciences,* 108**,** 452-461.

Sung, J. H., Ji, J. H., Song, K. S., Lee, J. H., Choi, K. H., Lee, S. H. & Yu, I. J. 2011. Acute inhalation toxicity of silver nanoparticles. *Toxicology and industrial health,* 27**,** 149-154.

Takács-Novák, K., Józan, M., Hermecz, I. & Szász, G. 1992. Lipophilicity of antibacterial fluoroquinolones. *International Journal of Pharmaceutics,* 79**,** 89-96.

Takahashi, H., Hayakawa, I. & Akimoto, T. 2003. The history of the development and changes of quinolone antibacterial agents. *Yakushigaku Zasshi,* 38**,** 161-179.

Tamboli, D. P. & Lee, D. S. 2013. Mechanistic antimicrobial approach of extracellularly synthesized silver nanoparticles against gram positive and gram negative bacteria. *Journal of hazardous materials,* 260**,** 878-884.

Tandogdu, Z. & Wagenlehner, F. M. 2016. Global epidemiology of urinary tract infections. *Current opinion in infectious diseases,* 29**,** 73-79.

Tippayawat, P., Phromviyo, N., Boueroy, P. & Chompoosor, A. 2016. Green synthesis of silver nanoparticles in aloe vera plant extract prepared by a hydrothermal method and their synergistic antibacterial activity. *PeerJ,* 4**,** e2589.

Ulaeto, S. B., Mathew, G. M., Pancrecious, J. K., Nair, J. B., Rajan, T., Maiti, K. K. & Pai, B. 2019. Biogenic Ag nanoparticles from neem extract: their structural evaluation and antimicrobial effects against Pseudomonas nitroreducens and Aspergillus unguis (NII 08123). *ACS Biomaterials Science & Engineering,* 6**,** 235-245.

Vaseghi, Z., Nematollahzadeh, A. & Tavakoli, O. 2018. Green methods for the synthesis of metal nanoparticles using biogenic reducing agents: a review. *Reviews in Chemical Engineering,* 34**,** 529-559.

Vila, J., Sáez-López, E., Johnson, J. R., Römling, U., Dobrindt, U., Cantón, R., Giske, C., Naas, T., Carattoli, A. & Martínez-Medina, M. 2016. Escherichia coli: an old friend with new tidings. *FEMS microbiology reviews,* 40**,** 437-463.

Vineetha, N., Vignesh, R. & Sridhar, D. 2015. Preparation, standardization of antibiotic discs and study of resistance pattern for first-line antibiotics in isolates from clinical samples. *International Journal of Applied Research,* 1**,** 624-631.

Walsh, C. & Collyns, T. 2017. The pathophysiology of urinary tract infections. *Surgery (Oxford),* 35**,** 293-298.

Who 2014. Antimicrobial resistance: global report on surveillance.

Who 2018. WHO report on surveillance of antibiotic consumption: 2016-2018 early implementation.

Willyard, C. 2017. The drug-resistant bacteria that pose the greatest health threats. *Nature News,* 543**,** 15.

Wright, G. D. 2011. Molecular mechanisms of antibiotic resistance. *Chemical communications,* 47**,** 4055-4061.

Wu, G., Wang, G., Fu, X. & Zhu, L. 2003. Synthesis, crystal structure, stacking effect and antibacterial studies of a novel quaternary copper (II) complex with quinolone. *Molecules,* 8**,** 287-296.

Wu, S., Zhang, B., Liu, Y., Suo, X. & Li, H. 2018. Influence of surface topography on bacterial adhesion: A review. *Biointerphases,* 13**,** 060801.

Zhang, X.-F., Liu, Z.-G., Shen, W. & Gurunathan, S. 2016. Silver nanoparticles: synthesis, characterization, properties, applications, and therapeutic approaches. *International journal of molecular sciences,* 17**,** 1534.

Zou, L., Wang, J., Gao, Y., Ren, X., Rottenberg, M. E., Lu, J. & Holmgren, A. 2018. Synergistic antibacterial activity of silver with antibiotics correlating with the upregulation of the ROS production. *Scientific reports,* 8**,** 11131.

7. APPENDICES

Appendix-1: Calibration curve of standard ciprofloxacin hydrochloride in distilled water at 275 nm

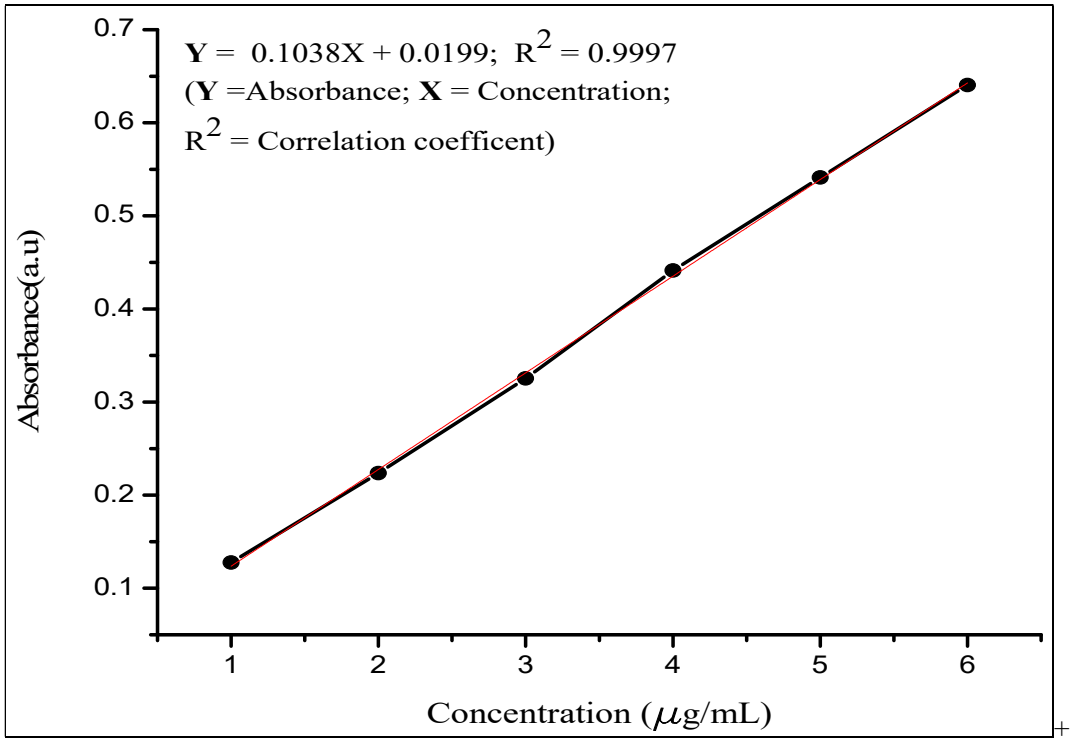

Appendix-2: Calibration graphs of standard ciprofloxacin hydrochloride at different λ-max for the corresponding pH medium: at 276 nm in pH 1.2 (A) and in pH 6 (B); at 270 nm in pH 6.8 (C) and at 268 nm in pH-7.4 medium

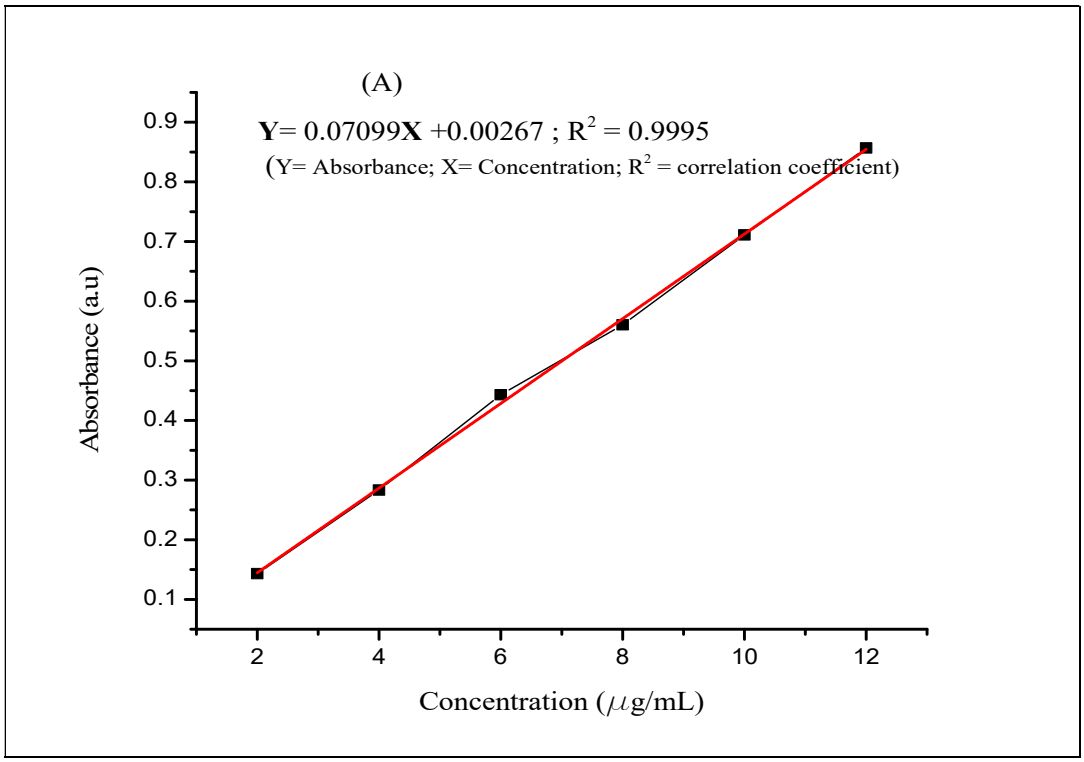

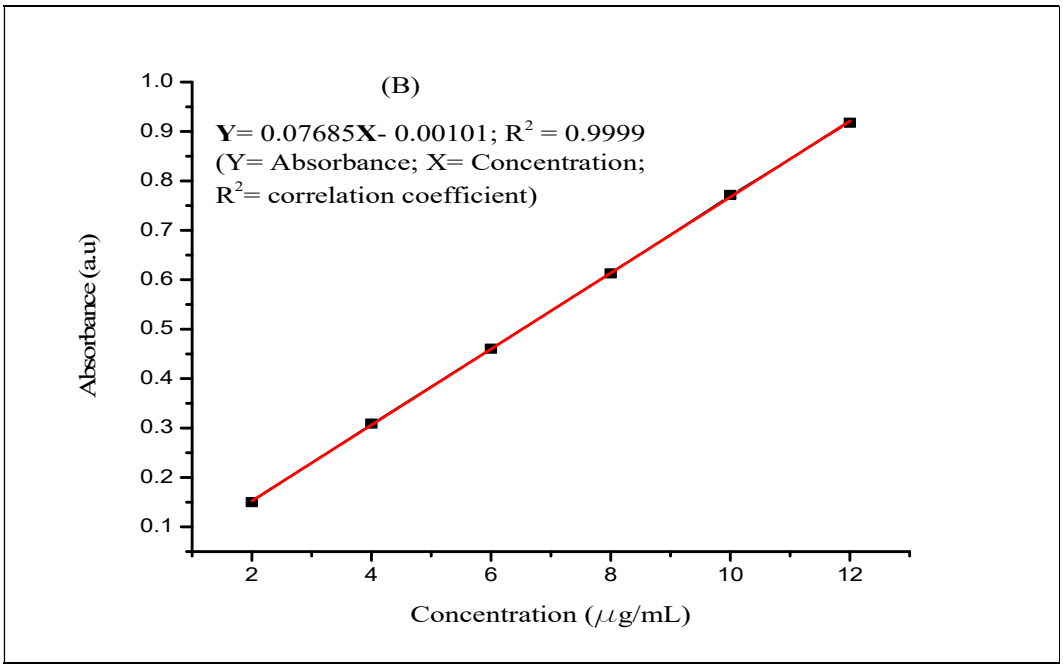

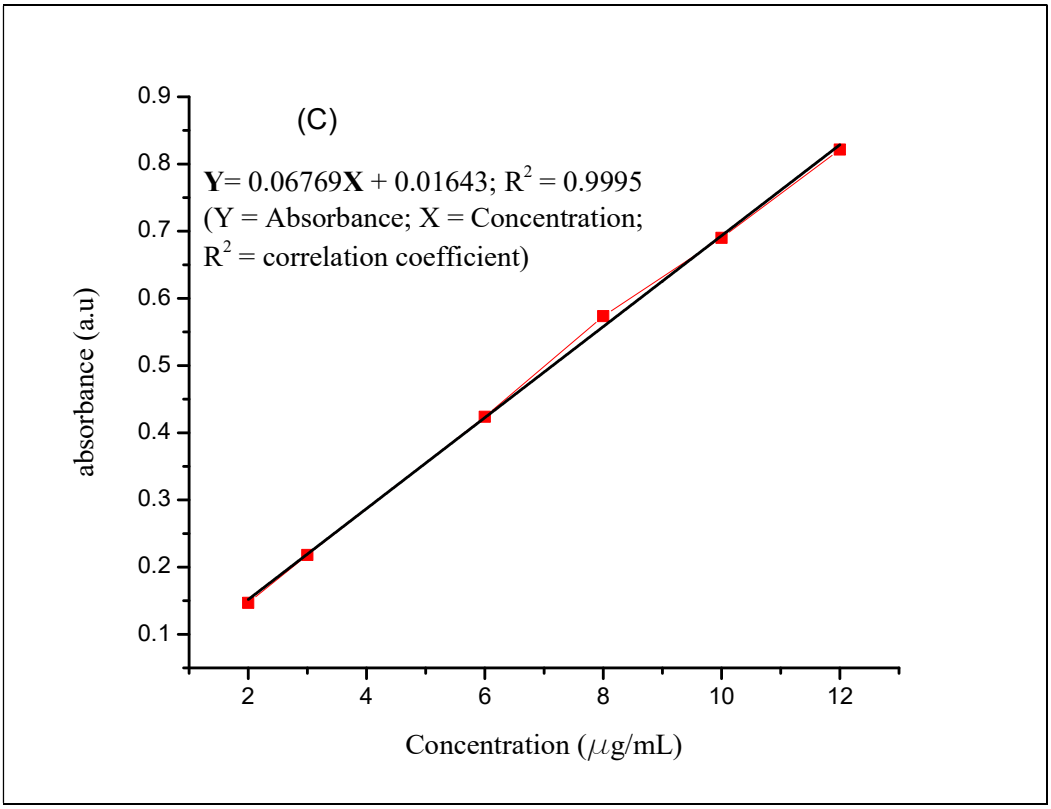
(C)
Y= 0.06769X + 0.01643; R2 = 0.9995
(Y = Absorbance; X = Concentration;
R2 = correlation coefficient)
absorbance (a.u)
Concentration (μg/mL)
0.9
0.8
0.7
0.6
0.5
0.4
0.3
0.2
0.1
2
4
6
8
10
12

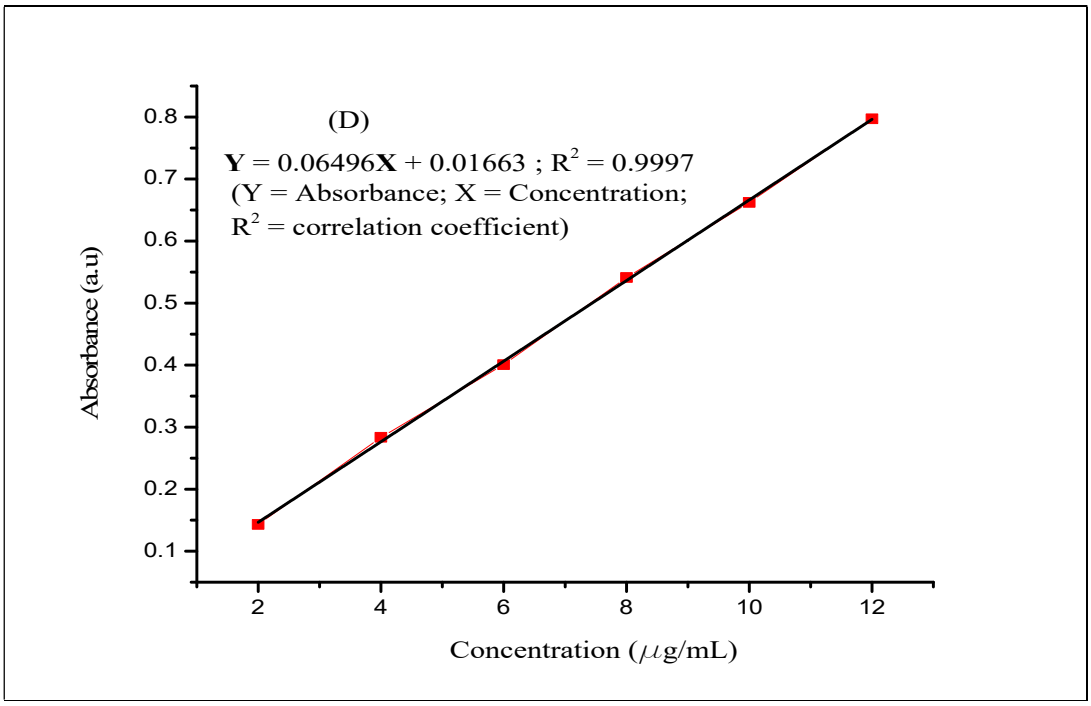
(D)
Y = 0.06496X + 0.01663 ; R2 = 0.9997
(Y = Absorbance; X = Concentration;
R2 = correlation coefficient)
Absorbance (a.u)
0.8
0.7
0.6
0.5
0.4
0.3
0.2
0.1
2
4
6
8
10
12
Concentration (μg/mL)